



## OPEN Predicting biomass global warming potential with FT-NIR spectroscopy

Prakash Gyawali<sup>1</sup>, Bijendra Shrestha<sup>2</sup>, Thitima Phanomsophon<sup>3</sup>, Jetsada Posom<sup>4</sup>✉, Pimpren Pornchaloempong<sup>5</sup>, Panmanas Sirisomboon<sup>1</sup>✉, Bim Prasad Shrestha<sup>2,6,7</sup> & Axel Funke<sup>8</sup>

This research is to predict the global warming potential (GWP) of biomass by using Fourier transform near-infrared (FT-NIR) spectroscopy. A partial least squares regression model of 197 biomass chip samples was developed for predicting GWP of fast-growing trees and agricultural residues. The reference value of GWP of biomass sample was calculated by the method provided by Intergovernmental Panel on Climate Change (IPCC). After applying different spectral pretreatments and variable selection methods, the best model for predicting GWP was found using the 1st derivative spectrum pretreatment and covariance method (COVM) based variable selection. The results indicate GWP model exhibit good predictive capabilities, where the model can be usable with caution for any purpose including research, by achieving a coefficient of determination for prediction set ( $R^2_p$ ) of 0.86, and ratio of prediction to deviation (RPD) of 2.6. Additionally, the RMSEP of 0.00063 suggests a low prediction error. This pioneering approach presents a swift and efficient means to determine GWP, the complex functionality parameter, which reveals an optimal relationship model, showcasing its efficacy in a significant advancement in the assessment of biomass functionality related to climate change issue. Additionally, the further research is recommended to integrate FT-NIR data with thermogravimetric analyser to simulate of different thermal conversion of biomass type where different emission gases are generated and with gas chromatography–mass spectrometry for evaluation of concentration of the generated gases for further refine GWP predictions which providing more comprehensive insights and exact content of emission gases affect global warming to support the IPCC.

**Keywords** Global warming potential, Climate change, Biomass emission, NIR

### Abbreviations

|      |                                   |
|------|-----------------------------------|
| C    | Carbon                            |
| CHNS | Elemental analyzer                |
| GA   | Geneticalgorithm                  |
| H    | Hydrogen                          |
| HHV  | Higher heating value              |
| LVs  | Latent variable number            |
| Max  | Maximum                           |
| Min  | Minimum                           |
| MP   | Multi-preprocessing               |
| MSC  | Multiplicative scatter correction |
| N    | Nitrogen                          |
| NT   | Total number of samples           |

<sup>1</sup>Department of Agricultural Engineering, School of Engineering, King Mongkut's Institute of Technology Ladkrabang, Bangkok 10520, Thailand. <sup>2</sup>Department of Mechanical Engineering, School of Engineering, Kathmandu University, PO Box 6250, Dhulikhel, Nepal. <sup>3</sup>Office of Administrative Interdisciplinary Program on Agricultural Technology, School of Agricultural Technology, King Mongkut's Institute of Technology Ladkrabang, Bangkok 10520, Thailand. <sup>4</sup>Department of Agricultural Engineering, Faculty of Engineering, Khon Kaen University, Khon Kaen 40002, Thailand. <sup>5</sup>Department of Food Engineering, School of Engineering, King Mongkut's Institute of Technology Ladkrabang, Bangkok 10520, Thailand. <sup>6</sup>Nepal technology Innovation Center, Kathmandu University, PO Box 6250, Dhulikhel, Nepal. <sup>7</sup>Department of BioEngineering, University of Washington, William H. Foege Building 3720, 15Th Ave NE, Seattle, WA 98195-5061, USA. <sup>8</sup>Institute of Catalysis Research and Technology (IKFT), Karlsruhe Institute of Technology (KIT), Hermann-Von-Helmholtz-Platz 1, 76344 Eggenstein-Leopoldshafen, Germany. ✉email: jetspo@kku.ac.th; panmanas.si@kmitl.ac.th

|         |   |
|---------|---|
| N       | Number of sample in corresponded set            |
| NIRS    | Near infrared spectroscopy                      |
| O       | Oxygen  |
| PLSR    | Partial least squares regression                |
| $R^2$   | Coefficient of determination                    |
| $R^2$   | Coefficient of determination of calibration set |
| $R^2_c$ | Coefficient of determination of prediction set  |
| RMSEC   | Root means square error of calibration set      |
| RMSEP   | Root means square error of prediction set       |
| RPD     | Ratio of prediction to deviation                |
| S       | Sulfur  |
| SD      | Standard deviation                              |
| SEC     | Standard error of calibration set               |
| SEL     | Standard error of laboratory                    |
| SEP     | Standard error of prediction set                |
| SNV     | Standard normal variate                         |
| SPA     | Successive projection algorithm                 |
| SW      | Selected wavenumber                             |
| wt.%    | Weight percentage                               |

The concept of global warming potential (GWP) serves as a comparative measure of the amount of heat a greenhouse gas traps in the atmosphere relative to the heat trapped by an equivalent mass of carbon dioxide. Consequently, the GWP factor of CO<sub>2</sub> is set at 1. GWP is typically calculated over specific time horizons of 20, 100, or 500 years<sup>1</sup>. Climate is characterized by mean air temperature, relative humidity, wind patterns, precipitation, and frequency of extreme weather events, typically measured at least thirty years<sup>2</sup>. Climate change represents the most significant global threat humanity primarily driven by atmospheric carbon emission<sup>3</sup>. Climate change can occur naturally due to variation in the Sun's energy or through persistent human activities, such as the emission of greenhouse gases, sulfate aerosol or black carbon or changes in the land use<sup>4</sup>. Examples of climate change include global warming and the increase severity and frequency of floods and drought in various part of the world over recent decades<sup>5</sup>. Climate change includes both natural variability and anthropogenic changes<sup>6</sup>. According to the Sixth Assessment Report (AR6 2021) by the Intergovernmental Panel on Climate Change (IPCC), human activities have warmed the atmosphere, ocean, and land<sup>7</sup>. The United Nations is concerned primarily with anthropogenic climate change, both because it poses a threat to global security and because it can be altered by altering human and governmental behavior. For this reason, the United Nation Framework of Climate Change defines climate change as a change of climate which is attributed directly or indirectly to human activity that alters the composition of the global atmosphere and which is in addition to natural climate variability observed over comparable time periods<sup>8</sup>. The international agreements overseen by the United Nations Framework Convention on Climate Change (UNFCCC), including the 1992 Kyoto Protocol and 2015 Paris climate agreement sought to build global consensus on fighting climate change and set clear goals for emission reductions<sup>9</sup>. The climate conference in Kyoto, Japan, resulted in an argument by industrialized nations to reduce emissions of six key greenhouse gases (GHGs) to about 5% below 1990 emissions level by the year 2012<sup>10</sup>. Reducing greenhouse gas emissions is one of the significant benefits of biomass. Biomass may function on a closed carbon cycle, in contrary to fossil fuels, which emit carbon dioxide stored for millions of years. This indicates that, when biomass is burned sustainably, the amount of carbon dioxide released during combustion is about equal to the amount absorbed by the plants during growth, leaving a net neutral effect on atmospheric CO<sub>2</sub> levels<sup>11</sup>. Additionally, biomass contributes to energy security through dedicated energy crops and municipal solid waste conversion, while stimulating economic development in rural areas by creating jobs and revitalizing economies. The integration of biomass with other renewables like solar and wind, coupled with ongoing technological advancements, improves efficiency and competitiveness, making it essential for achieving net zero emissions (NZE) of IEA (International Energy Agency, France) targets and addressing climate change<sup>12</sup>.

Biomass serves as a key renewable bio-resource, offering a carbon-neutral alternatives that is widely available across the globe<sup>13</sup>. Defined broadly, biomass encompasses all organic materials derived from plants, including algae, trees, and crops. The materials results from the process of photosynthesis, where green plants convert sunlight into organic matter<sup>14</sup>. Biomass includes terrestrial and aquatic vegetation as well as organic waste materials. The composition of biomass primarily consists of three polymers: cellulose, hemicellulose, and lignin, with variations contingent upon the specific type of biomass<sup>15</sup>. For instance, hardwood and herbaceous biomass contain approximately 43–47% and 33–38% cellulose, 25–35% and 26–32% hemicellulose and 16–24% and 17–19% lignin, respectively<sup>16</sup>. Biomass can be evaluated for its energy potential by analyzing its higher heating values (HHV) and ultimate analysis, which provides information on its elemental composition, including the percentage of carbon (C), hydrogen (H), nitrogen(N), sulfur (S), and oxygen (O). The HHV, measured using bomb calorimeter, is a crucial indicator of biomass energy content. Biomass with higher C and H, and/or O and H contents, and lower N and S contents, is preferable for energy use as enhances the HHV<sup>17</sup>. Biomass is highly responsive to Near Infrared (NIR) radiation, particularly indicated by spectra shown in the range of 1100 nm to 2500 nm<sup>17</sup>. It primarily interacts with hydrogen bonds in biological materials like C-H, O-H, N-H and S-H and C=O too. This property makes biomass suitable for assessment using Near Infrared Spectroscopy (NIRS) which combined NIR spectral variables to chemometric algorithms to determine energy-related properties such as HHV and elemental composition<sup>18</sup>, where provide rapid, non-destructive analysis with minimal or no sample preparation and no chemical used leading to environment safe. In the present scenario, biomass is one potential source of renewable energy and the conversion of plant material into a suitable form of energy, usually electricity

or as a fuel for an internal combustion engine, can be achieved using a number of different routes, each with specific pros and cons<sup>19</sup>. For carbondioxide (CO<sub>2</sub>) emission from biomass combustion though will be achieving net zero emissions (NZE) as explained, though, by GWP of CO<sub>2</sub> calculated by IPCC can be used for estimation of how much heat can be absorbed by biomass plants. For methane (CH<sub>4</sub>) and nitrous oxide (N<sub>2</sub>O), using Global Warming Potential (GWP) indices higher than those specified by the Kyoto Protocol (100-year time horizon) would better reflect historical temperature trends. The GWP of CH<sub>4</sub> aligns most accurately with historical temperature data when calculated over a 44-year time horizon. In contrast, the GWP of N<sub>2</sub>O does not closely match historical temperatures regardless of the time horizon used<sup>20</sup>. Hao and Ward<sup>21</sup> reported about 85% of the total CH<sub>4</sub> emitted in the tropical area, is mainly the result of shifting cultivation, fuelwood use, and deforestation and may have increased by at least 9% during the last decade because of increases in tropical deforestation and the use of fuelwood. There were some reports on N<sub>2</sub>O emissions by biomass burning e.g. from power generation using oil palm empty fruit branch was reported<sup>22</sup> and using rice husk<sup>23</sup>.

A complex pattern of peaks and troughs of NIR spectrum can be analyzed using chemometric techniques to deduce the sample's chemical composition and physical properties. The advantage of NIRS lies in its ability to provide rapid, non-destructive analysis with minimal or no sample preparation and no chemical used leading to environment safe. This makes it particularly valuable in fields such as agriculture, pharmaceuticals, and food industries, where it is used for quality control and compositional analysis.

Fourier Transform Near Infrared (FT-NIR) spectrometer is a analytical instrument that utilizes the NIR region to analyze materials. FT-NIR spectroscopy is a powerful analytical technique used for identifying and quantifying gases due to its high sensitivity and accuracy<sup>24</sup>. This method involves measuring the absorption of NIR radiation by gases, allowing for precise determination of their concentrations in the atmosphere. By integrating GWP estimation with FT-NIR spectroscopy, by result at the end of this report, it becomes possible to enhance the accuracy of greenhouse gas inventories and improve the reliability of climate models, thereby supporting more effective climate action.

The principle behind the IPCC's used the GWP calculation to quantify the impact of various green house gases (GHGs), mainly carbon dioxide (CO<sub>2</sub>), along with smaller amounts of methane (CH<sub>4</sub>) and nitrous oxide (N<sub>2</sub>O), on global warming relative to CO<sub>2</sub> is depended on the HHV which is the total energy content in the biomass, including the energy contained in the water vapor produced during combustion. It is important for estimating the potential emissions per unit of biomass. IPCC's GHG emissions estimation is calculated by using Emission Factor is a standard coefficient provided by IPCC guidelines, which estimates the amount of a specific greenhouse gas emitted per unit of energy produced by the biomass. The emission factors typically measure emissions in kilograms of CO<sub>2</sub>, CH<sub>4</sub>, or N<sub>2</sub>O per unit of energy (TJ) in the biomass, and they allow us to quantify the emission per unit of HHV. How much heat a gas traps in the atmosphere over a specific period, typically 20, 100 or 500 years, compared to CO<sub>2</sub>. This is based on the radiative efficiency of the gas (how effectively it absorbs heat per molecule) and its atmospheric lifetime (how long it remains in the atmosphere). CO<sub>2</sub> is set as the baseline (GWP=1) for comparison, as it is the most prevalent GHG emitted by human activities. Other gases are compared relative to CO<sub>2</sub>'s warming effect. GWP values depend on a chosen time horizon (e.g. GWP-20, GWP-100). Short lived gases, like CH<sub>4</sub>, have a higher GWP over a 20-year horizon due to their potent but shorter-lived impact, whereas the GWP-100 of CH<sub>4</sub> is lower because it dissipates faster than CO<sub>2</sub>. GWP represents the cumulative impact of a pulse emission over the chosen time horizon. The calculation integrates the warming effects of the gas over time, taking into account both the immediate warming effect and gradual decay of the gas. This method provides a standardized way to compare the warming impacts of different GHGs and is instrumental for climate policy, as it allows policymakers to prioritize mitigation efforts based on the long term and short-term impacts of various gases.

The database report presents developed models tailored for different biological materials, for example, the evaluation of HHV sorghum samples<sup>25</sup>, using partial least squares regression (PLSR) and principal component regression (PCR), calibration models were constructed for both full and reduced wavenumber regions to predict HHV and the contents of carbon, hydrogen, nitrogen, sulfur, and oxygen. Particularly noteworthy was the exceptional accuracy demonstrated by the HHV and carbon content models, underscoring their reliability in prediction and with a rapid measurement time (from 100 to 1 min)<sup>25</sup>. Predicting Global Warming Potential (GWP) using FT-NIR spectroscopy represents a novel approach. To develop the prediction model, the reference two key papers that utilize PLSR. There were two reports of our research group contributed to the results of NIR prediction models for ultimate analysis parameters of the non-wood and wood samples, including Pitak, Sirisomboon, Saengprachatanarug, Wongpichet, and Posom<sup>26</sup> who developed the PLSR using the spectra obtained by line-scan NIR hyperspectral imager in which the most effective model for the prediction of C, H and N content of 160 non-wood and wood biomass pellets The second report was contributed by Shrestha et al.<sup>17</sup> using FT-NIR spectrometry, where the ground non-wood and wood samples spectra, which were 110 samples of agricultural residues and 90 samples of fast growing trees, were used to develop the PLSR models combined with multi-preprocessing methods for ultimate analysis.

The prediction model that is applicable for determining the GWP for different species and utilized the species as for GWP production is essential for the policy makers, energy companies, and researchers who can utilize these findings for proper identification, management, and the utilization of resources to save the planet. Therefore, the main objective of this research is to propose a novel estimation approach for GWP by combined the GWP calculation method obtained from IPCC<sup>11</sup> which utilizing HHV of the biomass and FT-NIR spectra of biomass samples by formulating a PLSR prediction model which can drastically reduce the experiment period from 40 min for HHV measurement by bomb calorimeter include sample preparation time<sup>17</sup> to a reduction to 3 min by only use the spectrum of the biomass chips.

Traditional methods are time-consuming (40 min), chemical unavoidable (e.g. tablets of benzoic acid and combustion polyethylene bag) cause non-environmental friendly, well trained technician is required, costly (15

USD per sample) and destructive while FT-NIR offers a fast (3 min), chemical free cause environmental friendly, general worker can work, evaluation and operation cost per sample (< 1 USD) and non-destructive.

It is an AI approach to be an alternative instead of traditional method for estimating GWP from biomass, aiding sustainable biomass utilization and climate impact assessment. We believe readers will find this work insightful and valuable, as it introduces a rapid, non-destructive, and cost-effective approach for GWP assessment, addressing a critical gap in biomass analysis and climate change mitigation.

## Materials and methods

In this manuscript, we introduce a novel approach for predicting Global Warming Potential (GWP) using a spectroscopy non-destructive and rapid method but by using diverse biomass sources including fast growing tree and agricultural residue collected in Shrestha et al.<sup>17</sup>. In Shrestha et al.<sup>17</sup> only the higher heating value and ultimate analysis elements were predicted. To the best of our knowledge, no prior research has explored this specific application, making it a novel contribution to the field, especially in climate change environment sector.

This research is the longitudinal research and builds on the study referenced at Shrestha et al.<sup>17</sup> <https://doi.org/10.3390/en16145351>, where in previous paper traditional CHN/S elemental analyzer was used to determine elements such as C, N, O, and S, and bomb calorimeter was used for measuring HHV. Using of same sample spectrum set, we have developed a new model that offers an alternative approach to determining GWP and HHV data using PLSR. This streamlined model is designed to provide a faster and more accessible method for estimating GWP in biomass applications.

Figure 1 illustrates the comprehensive research methodology for assessing the HHV and GWP of ground biomass for energy applications, employing NIRS in conjunction with PLSR analysis.

### Biomass

Shrestha et al.<sup>17</sup> gathered Nepal biomass samples focusing on five fast-growing tree species: *Alnus nepalensis*, *Pinus roxburghii*, *Bambusa vulgaris*, *Bombax ceiba*, and *Eucalyptus* and five types of agriculture residues: *Zea mays* (cob, shell, and stover), *Oryza sativa* (husk), and *Saccharum officinarum* (bagasse). There were 200 samples in total.

Outliers in the GWP calculated data were identified using z-score equation in Eq. (1), which is the Z score and when the Z score is  $\geq 3$ , it means that the x value is outside the  $\pm 3SD$  range where 99.7% of data is and the x value will be considered as outlier<sup>27</sup>. x is the reference value of GWP,  $\bar{x}$  is the average GWP, and SD is the standard deviation. There were 3 outliers found.

$$\frac{X_i - \bar{X}}{SD} \geq | \pm 3 | \quad (1)$$

The spectral outlier samples were determined by using the Mahalanobis distance limit, based on the distribution of all calibration spectra, where a normal distribution, a one-sided limit is defined that covers a probability of 99.999%<sup>28</sup>. However, there was no spectral outlier found. Hence, 197 samples for modeling. The investigation is significant as it addresses biomass sample from both tree species and agricultural residues, offering a board understanding of the potential energy yields from two critical categories of biomass resources. The study sheds light on renewable energy opportunities that can be derived from diverse plant species and residues, each with its distinct chemical and structural characteristics.

### Spectroscopy scanning

Shrestha et al.<sup>17</sup> scanned biomass samples using an FT-NIR spectroscopy (MPA, Bruker, Germany) in diffuse reflectance mode with a rotating sample holder. The use of diffuse reflectance mode and the rotating mode holder was instrumental in achieving uniform sample exposure to the spectrometer beam, which is critical in analyzing heterogeneous materials like biomass. The study highlights the importance of proper background calibration and careful sample handling in obtaining accurate FT-NIR spectra ensuring that environmental factors such as humidity and temperature for no skew the results<sup>29</sup>.

### Wet-lab measurement

The complex nature of NIR absorbance data, it is essential to correlate it with reference values obtained from a standard laboratory method to ensure accuracy<sup>30</sup>. Accordingly, the reference data for the biomass samples, which included higher heating (HHV), were evaluated following the procedure outlined by Shrestha et al.<sup>17</sup> after scanning with an FT-NIR spectrometer. Prior to HHV measurement, the grinding process is crucial for it ensures uniform particle size, which in turn improves the consistency of the combustion process and enhances the precision of the calorimetric analysis. The using Bomb calorimeter to find the HHV is widely recognized for its reliability in determining the calorific value of various type of fuel, including biomass. The use of an automatic bomb calorimeter ensures precise temperature control during combustion, allowing accurate measurement of the energy content released by the samples. This data is crucial for understanding the potential of biomass as a renewable energy source and optimizing its use in various applications.

### Estimation of global warming potential and emission of greenhouse gas (GHG)

IPCC guidelines<sup>7,31</sup> was used to obtain main emission factors for CO<sub>2</sub>, CH<sub>4</sub>, and N<sub>2</sub>O from stationary biomass combustion on the 100 years based reported in AR6<sup>7</sup>. These emission factors are typically expressed in grams of gas per unit of fuel burned energy (e.g., CO<sub>2</sub> kg TJ<sup>-1</sup> of fuel). Calculate the emissions of CO<sub>2</sub>, CH<sub>4</sub>, and N<sub>2</sub>O from the biomass combustion using the following formula: where Emissions is the total amount of emissions produced (kg); Mass of sample is the total mass of a sample being burned (kg); High Heating Value is the Gross Calorific

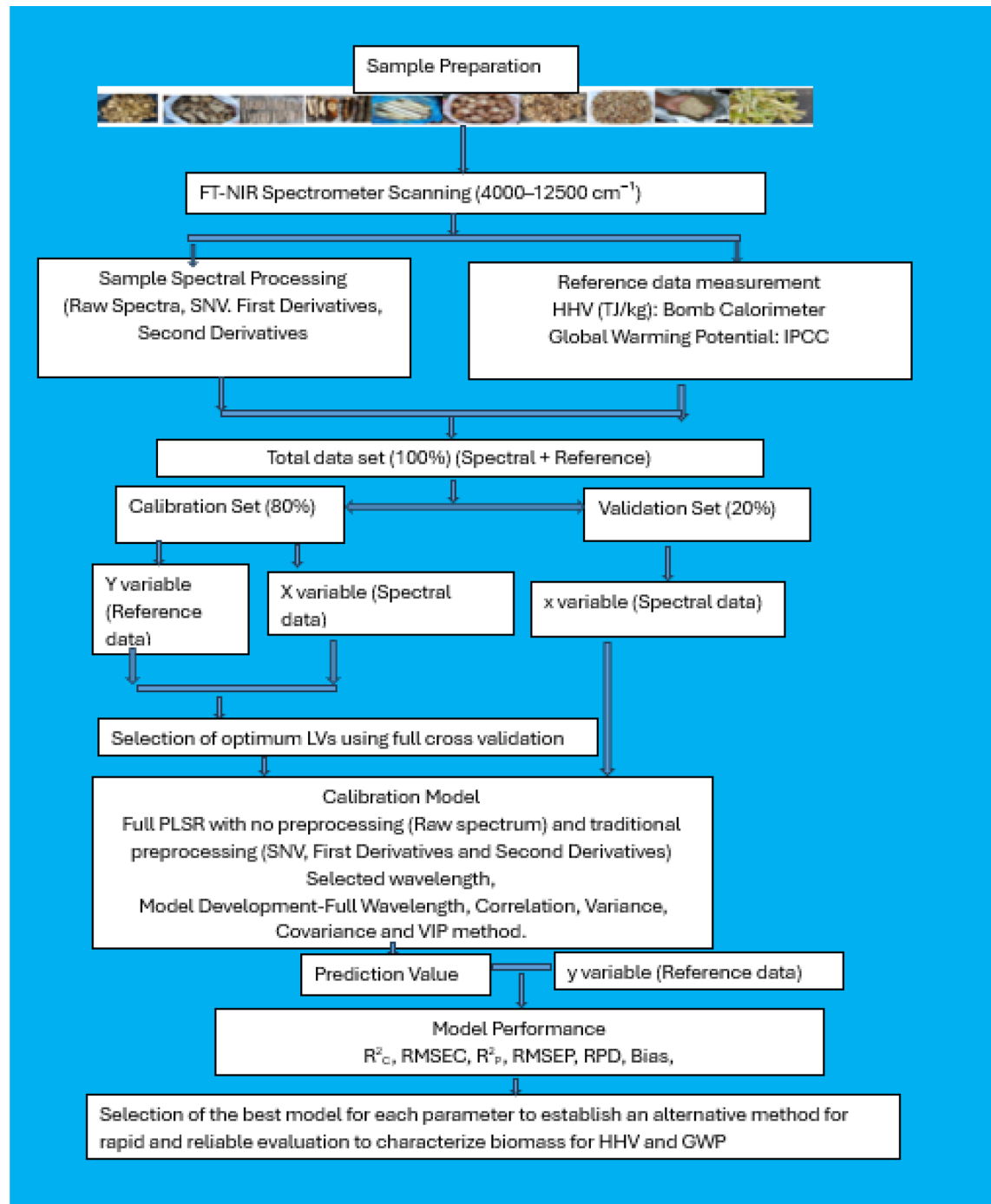


**Fig. 1.** Flow chart of the overall research methodology for the evaluation of the GWP by HHV using NIRS combined with PLSR.

Value, measures the total amount of energy that can be obtained from a fuel sample when it is completely burned (TJ.kg⁻¹); Emission Factor is based on energy consumption for wood/ woody residues: 112 kg CO<sub>2</sub> TJ⁻¹, 30 kg CH<sub>4</sub> TJ⁻¹, and 4 kg N<sub>2</sub>O TJ⁻¹<sup>17,31</sup>.

To determine the emission factor for biomass combustion, follow a systematic approach to ensure accuracy. Begin by identifying the type of biomass, such as fast-growing trees and agricultural residues, as each type has distinct emission factors. Reliable sources for these factors include the IPCC Guidelines. Next, measure the HHV of the biomass, often determined experimentally via bomb calorimetry and expressed in TJ kg⁻¹. Select an appropriate emission factor based on the biomass type and combustion conditions; for example, wood combustion factors range from 1 to 150 kg CO<sub>2</sub> TJ⁻¹.

Determine the GWP of the emissions using the IPCC's GWP values for a specific time horizon (e.g. 100 years). The GWP are calculated by converting the emissions of  $\text{CH}_4$  and  $\text{N}_2\text{O}$  into  $\text{CO}_2$ -equivalents ( $\text{CO}_2\text{e}$ ) based on their relative warming potential.

$$\text{GWP} = \frac{\int_0^a aicidt}{\int_0^a a\text{CO}_2\text{CCO}_2dt} \quad (2)$$

where  $ai$  is Absolute instantaneous concentration of the gas  $i$  at time  $t$ ;  $ci$  is Radiative efficiency (or radiative forcing) of the gas  $i$  per unit mass;  $a\text{CO}_2$  is Absolute instantaneous concentration of  $\text{CO}_2$  at time  $t$ ;  $cc\text{CO}_2$  is Radiative efficiency (or radiative forcing) of  $\text{CO}_2$  per unit mass;  $a$  is Time horizon over which the GWP is calculated 100 years (typically 20 or 100 years);  $t$  is Time variable.

The total GWP calculated the combined impact of different greenhouse gases (GHGs) on global warming. Each GHG has a specific GWP value, which represents its warming effect relative to  $\text{CO}_2$  over a specific time horizon, typically 100 years. For calculation, the total GWP is determined by summing the products of the GWP values and the emission quantities for each gas. Specifically, it includes the GWP of  $\text{CO}_2$  multiplied by the amount of  $\text{CO}_2$  emissions, the GWP of methane ( $\text{CH}_4$ ) multiplied by the amount  $\text{CH}_4$  emissions, and the GWP of nitrous oxide ( $\text{N}_2\text{O}$ ) emissions multiplied by the amount  $\text{N}_2\text{O}$  emissions. By accounting for the different contributions of these gases, the formula provides a comprehensive measure of the overall impact of multiple GHGs on climate change, allowing for a more accurate assessment of their collective influence on global warming.

For calculating GWP, use the formula:

$$\begin{aligned} \text{Step 1 : } & (\text{CO}_2, \text{CH}_4, \text{N}_2\text{O}) \text{ emissions (kg)} = \text{Mass of Fuel (kg)} \\ & \times \text{Carbon emission factor (kg TJ}^{-1}\text{)} \times \text{HHV (kg TJ}^{-1}\text{)} \end{aligned}$$

$$\begin{aligned} \text{Step 2 : Total GWP} & = (\text{GWP of CO}_2 \times \text{CO}_2 \text{ emissions}) \\ & + (\text{GWP of CH}_4 \times \text{CH}_4 \text{ emissions}) + (\text{GWP of N}_2\text{O} \times \text{N}_2\text{O} \text{ emissions}) \end{aligned}$$

Table 1 shows example of emission gases by *Alnus Nepalensis* biomass combustion.

| <i>Alnus nepalensis</i>  | Remarks   |
|--|---|
|  | IPCC guideline  |
| Calculation of $\text{CO}_2$ emission  |   |
| Higher Heating Value = 17,932,000 J $\text{kg}^{-1}$<br>$\text{CO}_2$ emission factor = 112 kg $\text{TJ}^{-1}$ ,<br>we can follow these steps:<br>Convert HHV to $\text{TJ kg}^{-1}$ :<br>Since 1 $\text{TJ} = 10^{12}$ J, we need to convert the HHV from $\text{J kg}^{-1}$ to $\text{TJ kg}^{-1}$ :<br>$\text{HHV in TJ kg}^{-1} = 17,932,000 \text{ J kg}^{-1} / 10^{12} = 1.7932 \times 10^{-3} \text{ TJ kg}^{-1}$  | $\text{CO}_2$ emission factor: 112 kg dry matter $\text{TJ}^{-1}$ (typical for wood combustion) |
| $\text{CO}_2$ emission (kg) = Mass of fuel (kg) $\times$ $\text{CO}_2$ emission factor (kg $\text{TJ}^{-1}$ ) $\times$ HHV (TJ $\text{kg}^{-1}$ )<br>$\text{CO}_2$ emission (kg) = 1 kg $\times$ 112 kg $\text{TJ}^{-1}$ $\times$ 0.017932 TJ $\text{kg}^{-1}$<br>Therefore, the $\text{CO}_2$ emission from stationary fuel combustion with an HHV of 17,932,000 J $\text{kg}^{-1}$ and using the default $\text{CO}_2$ emission factor of 112 kg $\text{TJ}^{-1}$ would be approximately $2.0083 \times 10^{-3}$ kg of $\text{CO}_2$ per kg of fuel  |   |
| Calculation of $\text{CH}_4$ emission  |   |
| High Heating Value = 17,932,000 J $\text{kg}^{-1}$<br>$\text{CH}_4$ emission factor = 30 kg $\text{TJ}^{-1}$<br>Convert HHV unit to $\text{TJ kg}^{-1}$<br>1 $\text{TJ} = 10^{12}$ J<br>HHV from $\text{J kg}^{-1}$ to $\text{TJ kg}^{-1}$ :<br>$\text{HHV in TJ kg}^{-1} = 17,932,000 \text{ J kg}^{-1} / 10^{12} = 1.7932 \times 10^{-5} \text{ TJ kg}^{-1}$   | $\text{CH}_4$ emission factor: 30 kg dry matter $\text{TJ}^{-1}$                                |
| $\text{CH}_4$ emission (kg) = Mass of Fuel (kg) $\times$ $\text{CH}_4$ emission factor (kg $\text{TJ}^{-1}$ ) $\times$ HHV (TJ $\text{kg}^{-1}$ )<br>$\text{CH}_4$ emission (kg) = 1 kg $\times$ 30 kg $\text{TJ}^{-1}$ $\times$ $1.7932 \times 10^{-5}$ TJ $\text{kg}^{-1}$<br>$\text{CH}_4$ emission (kg) = $5.3796 \times 10^{-4}$ kg of $\text{CH}_4$ per kg of fuel   |   |
| Calculation of $\text{N}_2\text{O}$ emission   |   |
| High Heating Value = 17,932,000 J $\text{kg}^{-1}$<br>$\text{N}_2\text{O}$ emission factor = 4 kg $\text{TJ}^{-1}$<br>Convert HHV unit to $\text{TJ kg}^{-1}$<br>1 $\text{TJ} = 10^{12}$ J<br>HHV from $\text{J kg}^{-1}$ to $\text{TJ kg}^{-1}$ :<br>$\text{HHV in TJ kg}^{-1} = 17,932,000 \text{ J kg}^{-1} / 10^{12} = 1.7932 \times 10^{-5} \text{ TJ kg}^{-1}$   | $\text{N}_2\text{O}$ emission factor 4 kg dry matter/ $\text{TJ}$                               |
| $\text{N}_2\text{O}$ emission (kg) = Mass of Fuel (kg) $\times$ $\text{N}_2\text{O}$ emission factor (kg $\text{TJ}^{-1}$ ) $\times$ HHV (TJ $\text{kg}^{-1}$ )<br>$\text{N}_2\text{O}$ emission (kg) = 1 kg $\times$ 4 kg $\text{TJ}^{-1}$ $\times$ $1.7932 \times 10^{-5}$ TJ $\text{kg}^{-1}$<br>$\text{N}_2\text{O}$ emission (kg) = $7.1728 \times 10^{-5}$ kg of $\text{N}_2\text{O}$ per kg offuel  |   |
| The concept of global warming potential (GWP) was introduced in IPCC –AR1 (Shine et al. 1990) to compare the greenhouse effects of different greenhouse gases relative to a reference gas, normally taken as carbon dioxide, under this definition, $\text{CO}_2$ would have a GWP value of 1<br><i>Alnus nepalensis</i><br>Total GWP = (GWP of $\text{CO}_2 \times \text{CO}_2$ emissions) + (GWP of $\text{CH}_4 \times \text{CH}_4$ emissions) + (GWP of $\text{N}_2\text{O} \times \text{N}_2\text{O}$ emissions)<br>Total GWP = $1 \times 2.0083 \times 10^{-3} + 29.8 \times 5.379 \times 10^{-4} + 273 \times 7.1728 \times 10^{-5}$<br>Total GWP = 0.0376 kg $\text{CO}_2\text{e}$<br>This calculation is by 100 years based GWP of emission gases followed AR6 <sup>7</sup> |   |

**Table 1.** Calculation example of emission gases by *Alnus nepalensis* biomass combustion.

The Table 2 shows the compares the GWPs of three greenhouse gases i.e.  $\text{CO}_2$ ,  $\text{CH}_4$ , and  $\text{N}_2\text{O}$ —over two different time periods (100 years and 20 years) based on assessments from the IPCC's Assessment Reports (AR4 2007<sup>32</sup>, AR5 2014<sup>33</sup>, and AR6 2021<sup>7</sup>). For  $\text{CO}_2$ , the GWP remains consistent across all reports and time periods with a value of 1, indicating its role as the baseline for comparison.  $\text{CH}_4$  shows variations in GWP depending on its origin (fossil or non-fossil) and whether climate-carbon feedback is considered. The GWP for fossil-origin  $\text{CH}_4$  increases from 25 in AR4 to 34 in AR6 over a 100-year period, highlighting the growing recognition of its impact. For non-fossil-origin  $\text{CH}_4$ , the GWP is slightly lower at 27.2 over 100 years in AR6. Over a 20-year period,  $\text{CH}_4$ 's GWP is significantly higher, emphasizing its short-term potency as a greenhouse gas.  $\text{N}_2\text{O}$  also shows variations, with its GWP slightly decreasing from AR4 to AR5 but increasing again in AR6, both over 100-year and 20-year periods. The data reflects the evolving understanding of the greenhouse effects of these gases, with updates in each assessment report based on the latest scientific research.

### Model development and validation

The PLSR method were used to develop the model. The samples were divided into calibration set (80%) and a prediction set (20%) by using Kennard-Stone method. Kennard-Stone data separation algorithm is based on an Euclidian distance calculation, where the sample with maximum distance to all other samples are selected, then the samples which are as far away as possible from the selected samples are selected, until the selected number of samples is reached<sup>34</sup>. This means that the samples are selected in such a way that they will uniformly cover the complete sample space, reducing the need for extrapolation of the remaining samples<sup>34</sup>. Initially, the model was developed using raw spectra, standard normal variate (SNV), 1st derivative and 2nd derivative transformations. The model was optimized by selecting wavenumbers through various variable selection methods, including the Correlation Method (CM), Variance Method (VM), Co-Variance Method (COVM), and Variable Importance Projection (VIP). The spectral data were pretreated using raw spectra, standard normal variate (SNV), as well as first derivative and second derivative transformations. The following spectra pretreatment methods: Standard Normal Variate (SNV) is for corrects scatter effects and baseline variations<sup>35</sup>, 1st and 2nd Derivative enhances spectral resolution by removing baseline shifts and emphasizing key spectral features, leading to better signal clarity<sup>35</sup>.

Feature selection methods: Correlation-based selection identifies the most relevant spectral variables by assessing their relationship with dependent variable which in our case is GWP and HHV; VIP prioritizes key spectral features that significantly contribute to the PLSR model, enhancing predictive accuracy, VM selects variables based on their variance, ensuring only features with significant variation are retained and COVM identifies variables with strong covariance relationships, helping in feature reduction while preserving important predictive information<sup>36</sup>.

MATLAB-R2020b (MathWorks, Natick, MA, USA) was used for both spectrum pretreatment and model development. The calibration model's performance was assessed using the coefficient of determination ( $R^2_c$ ) and root mean square error of calibration (RMSEC).

The obtained model was validated using the prediction set, and their performance was evaluated based on coefficient of determination of prediction ( $R^2_p$ ), root mean square error of prediction (RMSEP), bias and the ratio of prediction of deviation (RPD).

These parameters were calculated as follows, where  $y$  is the measured value,  $\hat{y}$  is the predicted value,  $i$  is subscript used to indicate the number of the sample,  $\bar{y}$  is mean of the measured value,  $N$  is the number of samples in respective set, and SD is the standard deviation of the measured values of the prediction set:

$$R^2_c, R^2_p = 1 - \frac{\sum (y_i - \hat{y}_i)^2}{\sum (y_i - \bar{y}_i)^2} \quad (3)$$

$$\text{RMSEC, RMSEP} = \sqrt{\frac{\sum_{i=1}^N (y_i - \hat{y}_i)^2}{N}} \quad (4)$$

$$\text{RPD} = \frac{\text{SD}}{\text{RMSEP}} \quad (5)$$

$$\text{Bias} = \frac{\sum_{i=1}^N (y_i - \hat{y}_i)}{N} \quad (6)$$

| Greenhouse Gas                  | 100-year time period  |          |          |                   | 20-year time period   |          |          |                   |
|---------------------------------|-----------------------|----------|----------|-------------------|-----------------------|----------|----------|-------------------|
|                                 | AR4 2007              | AR5 2014 | AR6 2021 |                   | AR4 2007              | AR5 2014 | AR6 2021 |                   |
|                                 | Feedback not included |          |          | Feedback included | Feedback not included |          |          | Feedback included |
| $\text{CO}_2$                   | 1                     | 1        | 1        | 1                 | 1                     | 1        | 1        | 1                 |
| $\text{CH}_4$ fossil origin     | 25                    | 28       | 34       | 29.8              | 72                    | 84       | 86       | 82.5              |
| $\text{CH}_4$ non fossil origin |                       |          |          | 27.2              |                       |          |          | 80.8              |
| $\text{N}_2\text{O}$            | 298                   | 265      | 298      | 273               | 289                   | 264      | 268      | 273               |

**Table 2.** Global warming potential (GWP) of greenhouse gas emissions indicated in IPCC AR6 report<sup>7</sup>.

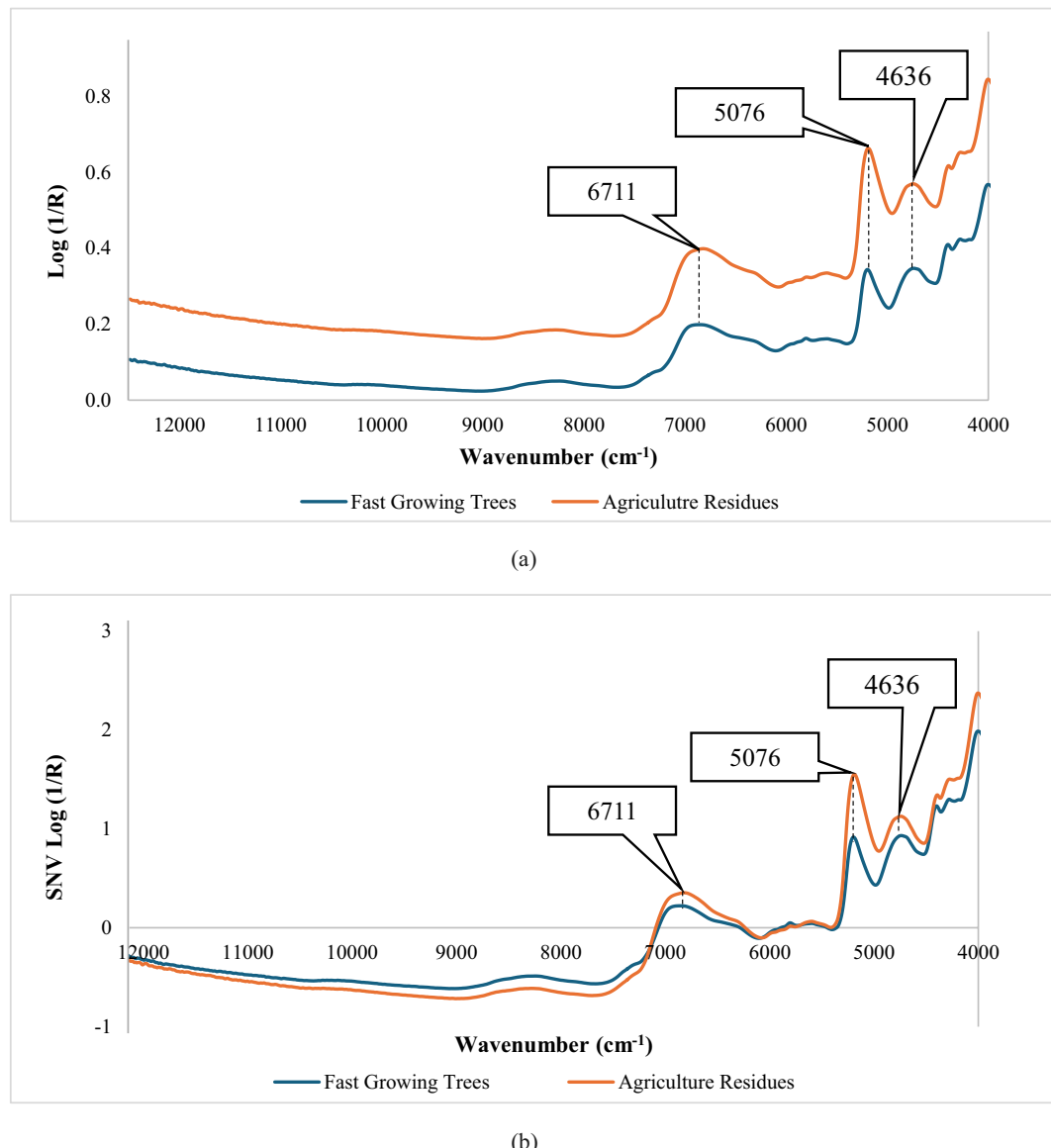


**Fig. 2.** Spectra of biomass chips of fast-growing trees and agricultural residue: raw (a) and pretreated spectra by SNV (b), 1st derivative (c) and 2nd derivative (d) where (a) raw spectra showing unprocessed near-infrared (NIR) data with baseline variations and scattering effects. (b) Standard Normal Variate (SNV) corrected spectra, reducing baseline shifts and scattering effects. (c) 1st derivative corrected spectra, to obtain common spectra baseline. (d) 2nd derivative corrected spectra, to obtain common spectra baseline and reveal overlapping peaks.

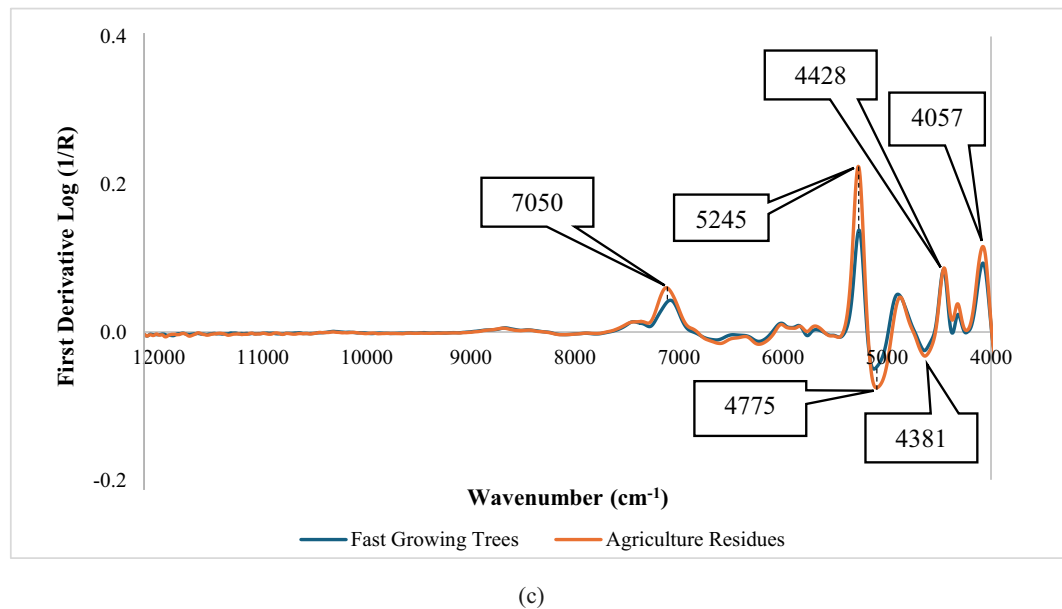
The better model was selected based on the tradeoff value between the highest  $R^2_{C}$ ,  $R^2_{P}$  and RPD and lowest RMSEC, RMSEP, and bias. In this study, the performance result, namely the  $R^2$  and RPD value were interpreted based on the recommendations of Williams et al.<sup>37</sup>.

## Result

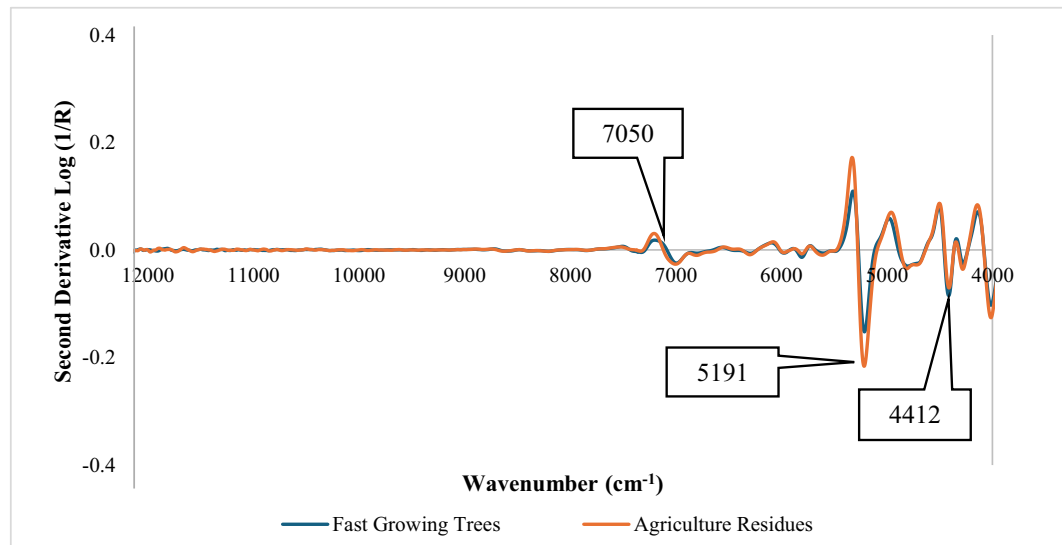
### Spectral data processing

In data of 200 biomass samples for GWP PLSR modeling, 3 outliers were identified and removed, resulting in a final dataset of 197 samples. The removal of outliers ensured the genuine performance of the model, allowing for more accurate predictions.

Figure 2a illustrates the raw spectra of log (1/R) versus wavenumber in the range of 3600–12500 cm<sup>-1</sup>, showing high absorption peak such as 6711, 5076 and 4636 cm<sup>-1</sup> for both fast growing tree and agriculture residues sample. It shows the significant absorption features corresponding to various molecular vibrations in the biomass. The peak at 6711 cm<sup>-1</sup> (1490 nm) of the broad band can be the shifted peak of 1471 nm is the first overtone of N-H stretching of CONH<sub>R</sub> typically found in amides or proteins and or 1450 nm attributed to 1st overtone of O-H vibration including of water and starch<sup>38,39</sup>. The combustion of starch is a significant process,



(c)



(d)

**Fig. 2.** (continued)

as it releases carbon dioxide ( $\text{CO}_2$ ), a major greenhouse gas that contributes to global warming<sup>40–42</sup> for example in biomass combustion, though, it is carbon neutral fuel.

The peak at  $5076 \text{ cm}^{-1}$  (1970 nm) is the shifted peak of  $1940 \text{ nm}$  is linked to O-H combination of fundamental of O-H stretching and bending vibrations<sup>38</sup>. The peak of  $4636 \text{ cm}^{-1}$  (2157 nm) corresponds to C-H aromatic C-H<sup>38</sup>. The wavenumber increases beyond  $6000 \text{ cm}^{-1}$  shows the flat spectral lines without dominant peaks, suggesting in the biomass a very less bond vibration in the wavenumber range due to NIR absorption.

Posom et al.<sup>43</sup> indicated the similar peaks for milled bamboo which is solely one species of biomass where the main peaks were  $6823 \text{ cm}^{-1}$  (1466 nm),  $5192 \text{ cm}^{-1}$  (1926 nm),  $4752 \text{ cm}^{-1}$  (2104 nm) and  $3992 \text{ cm}^{-1}$  (2505 nm). These indicate the influence of different kinds of biomass species on average spectrum.

Figure 2b shows the absorbance spectra pretreated using SNV transformation. A similar peak structure of raw spectrum is maintained in SNV spectrum. However, SNV preprocessing effectively mitigates baseline shifts, enhancing spectral comparability. Although both sample types exhibit similar spectral characteristics, but the main peaks after  $12,500\text{--}6000 \text{ cm}^{-1}$  the absorption of agricultural residue exhibit higher, including the range between  $4397 \text{ cm}^{-1}$  (2274 nm, lignin vibration) and  $4011 \text{ cm}^{-1}$  (2493 nm, lignin and cellulose vibration)<sup>44</sup> and near to  $4755 \text{ cm}^{-1}$  (2103 nm) is the band for  $\alpha$ -d- glucose, and  $4000 \text{ cm}^{-1}$  (2500 nm) is the band corresponding to C-H stretching + C-C stretching of starch<sup>39</sup>. But the vibration of between  $6000\text{--}5600 \text{ cm}^{-1}$  which is broad weak

band of lignin and cellulose where the peak  $5951\text{ cm}^{-1}$  (1680 nm) is the peak of pure lignin<sup>43</sup>, the band of both species is very close absorption. Though, beyond  $6000\text{ cm}^{-1}$  the absorption is lower obviously.

Figure 2c shows the plot of the 1st derivative of  $\log(1/R)$  versus wavenumber that reveals distinct spectral features. Significant peaks were observed in the  $4000$  to  $7000\text{ cm}^{-1}$  range, with the most prominent peaks around  $7050$ ,  $5245$ ,  $4775$ ,  $4428$ ,  $4381$  and  $4057\text{ cm}^{-1}$ . Specifically, the peak at  $7050\text{ cm}^{-1}$  is related to C–H combination bands found in hydrocarbons or aromatic<sup>38</sup>. The peak at  $5245\text{ cm}^{-1}$  relates with P–OH groups in phosphate<sup>38</sup>. The peak at  $4775\text{ cm}^{-1}$  corresponds to the O–H deformation band, which is present in alcohol or water<sup>38</sup>. The peak at  $4428\text{ cm}^{-1}$  represents lignin<sup>38</sup>. The peak at  $4381\text{ cm}^{-1}$  corresponds to C–H stretching and  $\text{CH}_2$  deformation bending in polysaccharides<sup>38</sup>. The peak  $4057\text{ cm}^{-1}$  corresponds to the  $\text{CONH}_2$  groups commonly present in proteins<sup>38</sup>. These peaks indicate the rapid change absorption points in raw spectra at these wavenumbers. Beyond  $7000\text{ cm}^{-1}$ , the data trend stabilizes, showing minimal variations up to  $12500\text{ cm}^{-1}$ . This stabilization suggests very low and consistent absorption characteristics in the higher wavenumber range. The zero absorption in 1st derivative spectrum is the peak absorption in raw spectrum.

Figure 2d shows the 2nd derivative plot of  $\log(1/R)$  versus wavenumber providing insights to reveal the overlapping peaks in the raw absorption spectra and due to the gap of derivative, the shifted peaks of  $6711\text{ cm}^{-1}$  (1490 nm),  $5951\text{ cm}^{-1}$  (1680 nm),  $5076\text{ cm}^{-1}$  (1970 nm), near to  $4755\text{ cm}^{-1}$  (2103 nm),  $4636\text{ cm}^{-1}$  (2157 nm),  $4397\text{ cm}^{-1}$  (2274 nm),  $4011\text{ cm}^{-1}$  (2493 nm), and  $4000\text{ cm}^{-1}$  (2500 nm) in raw and SNV spectra are shown.

### Statistic values of GWP and HHV

The provided data in Table 3 comprehensively details the statistical analysis used in the development of a PLSR model. It shows that the GWP parameter in calibration set includes 148 samples. The values range from a maximum of 0.0390 to a minimum of 0.0330, with a mean of 0.0330 and an SD of 0.0012. The SD is approximately 36.4 times less than the mean (0.0330/0.0012), suggesting that the data points are closely clustered around the mean value. The prediction set of 50 samples is designed to test the accuracy and precision of the model developed using the calibration data set. For the GWP parameter, the prediction set samples have a slightly lower maximum, minimum and mean value and a higher SD of 0.0030 shows greater variability in the prediction set data compared to the calibration set.

The HHV ( $\text{J g}^{-1}$ ) statistics in the prediction set has slightly lower variation than the calibration set with SD of 836  $\text{J g}^{-1}$  compared to 848  $\text{J g}^{-1}$  indicating the same distribution of data.

### Predicting performance of biomass GWP using PLSR

GWP is a critical metric for assessing the environmental impact of various biomass. Accurate prediction of GWP can inform sustainable practices and policy decision. In this study, the PLSR method is utilized to model and predict the GWP of different biomass samples including fast growing trees and agricultural residue.

Table 4 shows the results for predicting GWP of various biomass developed from raw spectra and different spectra pre-treatment and different number of wavenumbers from the respective feature variable selection method, demonstrating by the number of latent factors,  $R^2_C$ , RMSEC,  $R^2_p$ , RMSEP, RPD and Bias. The prediction results depended on the development methods, spectral pre-treatment, and the number of wavenumbers. The models with different variable selection methods gave the same performance, but the number of wavenumbers differed. The model developed with CM (reduction of 1150 wavenumber of full range to 325 wavenumber) of 1<sup>st</sup> derivative spectra, gave best performance with  $R^2_p$  was 0.87 (Table 4).

In the context of predicting GWP of biomass using FT-NIR spectroscopy, the following Williams et al.<sup>37</sup> indicated  $R^2$  showed the proportion of the variance of the NIRS predicted data, i.e. GWP can be explained by the spectral variables or  $\log 1/R$  and shows the degree of which the predicted data can be change, for a given change in the spectral data which higher values of  $R^2$  indicating better predictive accuracy.

Figure 3 illustrates the scatter plot of the GWP of biomass calculated using IPCC method and predicted by NIRS using the 1<sup>st</sup> derivative of the 325 wavenumbers obtained by COVM which outperformed the other predictive model's performance of GWP. The COVM variable reduction method helps identify and retain the most relevant wavenumber, enhancing the model's efficiency and accuracy. The  $R^2_C$  and  $R^2_p$  of featured wavenumber selection model was 0.92 and 0.85, respectively, indicating a linear relationship between the predicted and calculated values during both the calibration and prediction. From Table 4 the RMSEC is 0.00053, and RMSEP is 0.00063 show low prediction errors. The bias, which measures the systematic error, is -0.00014, showing minimal deviation from zero and thus negligible bias in the predictions. The RPD value of 2.6 signifies a fair predictive capability of the model for functional parameter including GWP, as values 2.5–2.9 were considered for screening applications<sup>37</sup>. This method effectively enhances average the model's performance by focusing on the most informative wavenumber prediction and reducing dimensionality, leading to more accurate and reliable predictions. These high  $R^2_p$  values (0.85) in predicting the GWP indicate the model usable with caution for most application including research which the threshold of  $R^2$  indicated by Williams guidelines is between 0.83–0.90<sup>37</sup>.

| Parameter                 | Method           | NT  | Calibration set |         |         |         |         | Prediction set |          |          |         |         |
|---------------------------|------------------|-----|-----------------|---------|---------|---------|---------|----------------|----------|----------|---------|---------|
|                           |                  |     | NC              | Max     | Min     | Mean    | SD      | NP             | Max      | Min      | Mean    | SD      |
| GWP                       | IPCC guidelines  | 197 | 147             | 0.03905 | 0.03080 | 0.03564 | 0.00180 | 50             | 0.038943 | 0.033002 | 0.03577 | 0.00165 |
| HHV ( $\text{J g}^{-1}$ ) | Bomb calorimeter | 197 | 147             | 18,616  | 16,405  | 16,976  | 910     | 50             | 17,950   | 15,268   | 17,051  | 787     |

**Table 3.** Statistic values of GWP and HHV for modeling.

| Variable selection method | Spectral pretreatment | Number of wavenumber | Factor | Calibration set |                | Prediction set |                |                 | RPD |
|---------------------------|-----------------------|----------------------|--------|-----------------|----------------|----------------|----------------|-----------------|-----|
|                           |                       |                      |        | $R^2_c$         | RMSEC          | $R^2_p$        | RMSEP          | Bias            |     |
| Full wavelength           | Raw                   | 1150                 | 10     | 0.80            | 0.00054        | 0.76           | 0.00061        | -0.0004         | 2.7 |
|                           | SNV                   | 1150                 | 8      | 0.90            | 0.00053        | 0.82           | 0.00065        | -0.0007         | 2.5 |
|                           | FstDev                | 1150                 | 9      | 0.89            | 0.00055        | 0.82           | 0.00062        | -0.0006         | 2.6 |
|                           | SecDev                | 1150                 | 9      | 0.87            | 0.00054        | 0.84           | 0.00062        | -0.0004         | 2.6 |
| CM                        | Raw                   | 220                  | 10     | 0.80            | 0.00054        | 0.76           | 0.00063        | -0.0002         | 2.6 |
|                           | SNV                   | 220                  | 8      | 0.92            | 0.00053        | 0.80           | 0.00062        | -0.0004         | 2.6 |
|                           | FstDev                | 325                  | 9      | 0.91            | 0.00054        | 0.74           | 0.00068        | -0.0003         | 2.4 |
|                           | SecDev                | 555                  | 9      | 0.89            | 0.00053        | 0.83           | 0.00062        | -0.0005         | 2.6 |
| VM                        | Raw                   | 520                  | 10     | 0.93            | 0.00065        | 0.80           | 0.00071        | -0.00005        | 2.3 |
|                           | SNV                   | 795                  | 8      | 0.79            | 0.00082        | 0.85           | 0.00061        | -0.00004        | 2.7 |
|                           | FstDev                | 590                  | 9      | 0.91            | 0.0006         | 0.74           | 0.00083        | -0.00006        | 1.9 |
|                           | SecDev                | 885                  | 9      | 0.89            | 0.0006         | 0.82           | 0.00061        | -0.00003        | 2.6 |
| COVM                      | Raw                   | 510                  | 10     | 0.89            | 0.00061        | 0.82           | 0.00063        | -0.00071        | 2.6 |
|                           | SNV                   | 895                  | 8      | 0.95            | 0.00039        | 0.78           | 0.00076        | -0.00011        | 2.1 |
|                           | FstDev                | 325                  | 9      | 0.92            | <b>0.00053</b> | 0.85           | <b>0.00063</b> | <b>-0.00014</b> | 2.6 |
|                           | SecDev                | 450                  | 9      | 0.92            | 0.00053        | 0.81           | 0.00071        | 3.4553e-05      | 2.3 |
| VIP                       | Raw                   | 950                  | 10     | 0.80            | 0.00084        | 0.76           | 0.00062        | -0.00014        | 2.6 |
|                           | SNV                   | 850                  | 8      | 0.78            | 0.00084        | 0.84           | 0.00063        | -0.00011        | 2.6 |
|                           | FstDev                | 750                  | 9      | 0.91            | 0.00053        | 0.74           | 0.00083        | -0.00012        | 1.9 |
|                           | SecDev                | 985                  | 9      | 0.89            | 0.00061        | 0.82           | 0.00068        | -5.1928e-05     | 2.4 |

**Table 4.** Prediction of GWP of biomass of fast-growing tree and agriculture residue by PLSR. N: Number of samples in calibration set,  $R^2_c$ : coefficient of determination of calibration set, n: number of samples in prediction set,  $R^2_p$ : coefficient of determination of prediction set, RPD: ratio of prediction to deviation, CM: correlation method, VM: variance method, COVM: co-variance method, VIP: variable. Significant values are in [bold].

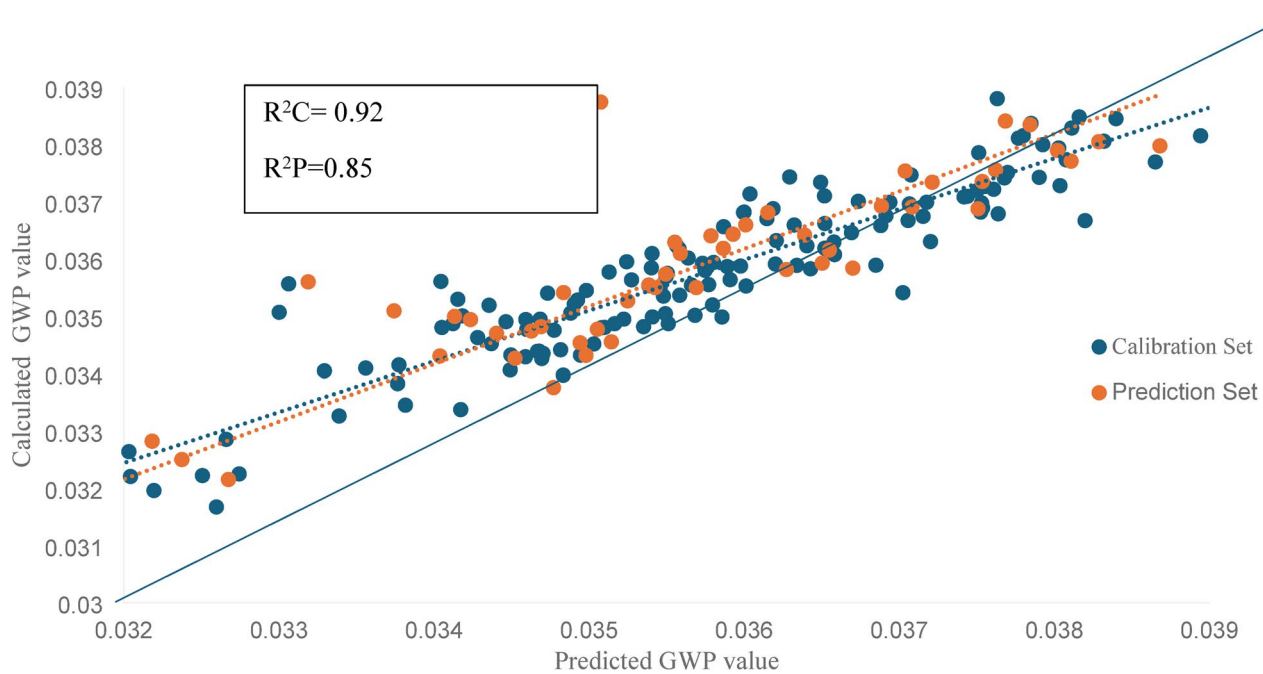


**Fig. 3.** IPCC calculated GWP versus NIRS predicted GWP in calibration and prediction sets. This PLSR modeling based on the first derivative spectra of 325 selected wavenumbers by covariance method, which demonstrated superior predictive performance compared to other models ( $R^2_c = 0.92$ ,  $R^2_p = 0.85$ ).

### Prediction result of HHV using PLSR

Table 5 displays the optimal result of PLSR-based models using the full wavenumber range (3600–12,500 cm<sup>-1</sup>) to evaluate the HHV of the chip biomass from the fast-growing trees and agricultural residues. Shrestha et al.<sup>17</sup> has described the HHV of the grounded biomass measured using the isoperibol method with an automatic bomb calorimeter (IKA C 200, Staufen, Baden-Württemberg, Germany). The data presents the performance of various pre-processing techniques—Raw Spectra, SNV, First Derivative, and Second Derivative—across calibration and prediction sets. Key metrics such as the number of latent factors,  $R^2_C$  and  $R^2_p$ , RMSEP, bias, and RPD were provided. Among these techniques, SNV demonstrates the highest  $R^2_C$  and  $R^2_p$ , though the value were low i.e.  $R^2_C$  (0.5879) and  $R^2_p$  (0.4972) values, indicating that while SNV provides some improvement in model performance compared to other preprocessing methods, the overall predictive capability of the model remains limited<sup>26</sup>. Additionally, SNV exhibits the lowest SEP (1.44 J g<sup>-1</sup>) and RMSEP (2.88 J g<sup>-1</sup>) values, suggesting more precise and accurate predictions compared to other techniques, though the  $R^2_p$  is very low making the model is not recommended to be used.

Figure 4 shows the best model for predicting the HHV of biomass was developed using the 2nd derivative spectra and variable selection by the COVM method. This approach reduced the number of variables from 1150 to 365 wavenumbers, significantly enhancing the model's performance ( $R^2_C$  of 0.98 and  $R^2_p$  of 0.87) indicating the model usable with caution for most application including research in predicting the HHV, and RPD value of 2.7 signifies a fair predictive capability of the model for functional parameter including GWP, as values 2.5–2.9 were considered for screening applications<sup>37</sup>.

### Regression coefficient and x-loading of GWP model

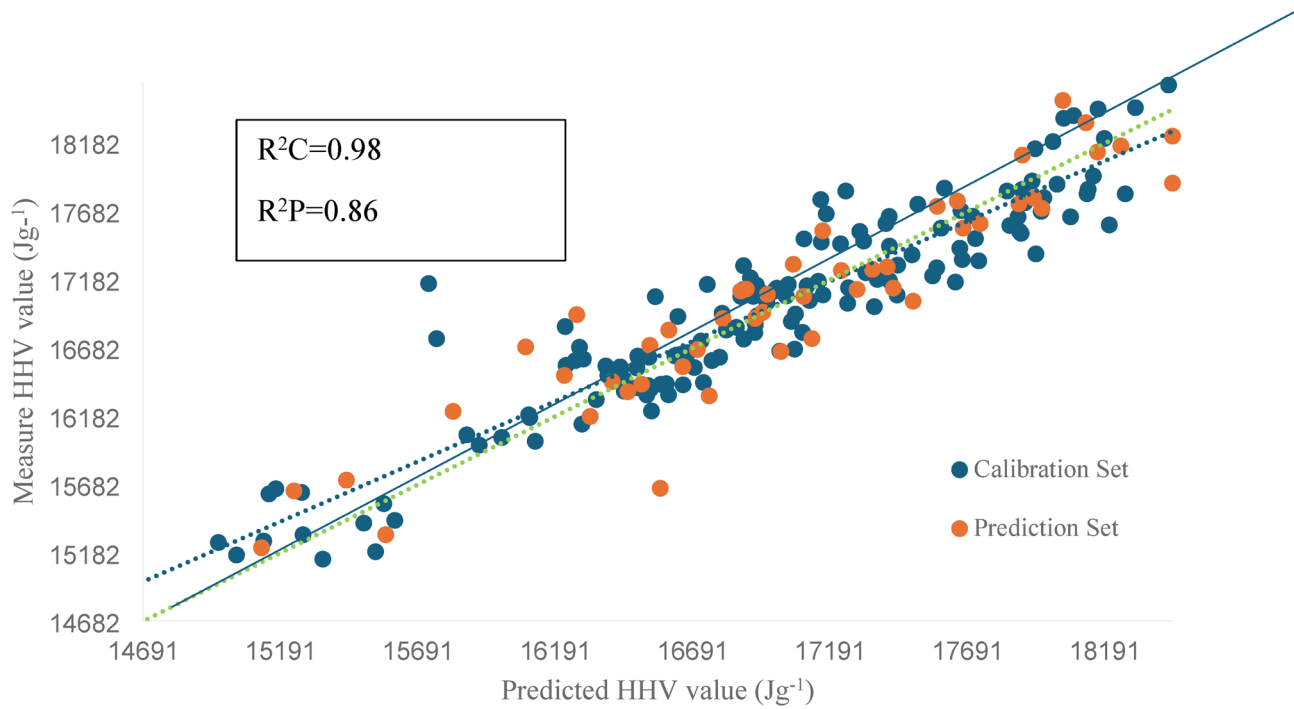
Prominent peaks were identified and the bond vibration interpretation is shown in Table 7 and the vibration indicated by Workman and Weyer<sup>38</sup> at the wavenumbers in bold were not found or not related to biomass.

Figure 5a presents the regression coefficient plot for the optimal PLS model predicting the GWP in biomass using the full-range wavenumber spectra. Prominent peaks were found at 4011 (Cellulose), 4196 [C-H (1v) + C-H (18)], 4651 [C-H (1v) + C-C (1v)], 4744, 5214 (water), 5400, 6001, 6086, 6441 (water) and 7151 [CH<sub>3</sub> (2v) + CH<sub>3</sub> (18)] cm<sup>-1</sup>. In comparison, the regression coefficient plot for the selected wavenumber model (Fig. 5b) revealed key peaks at 4142 [C-H (1v) + C-H (18)], 4389 [C-H (1v) + CH<sub>2</sub> (18)], 4605 proteins, 4867 amides/proteins, 5338, 6017, 7097, 7189 [CH<sub>3</sub> (2v) + CH<sub>3</sub> (18)] and 8686 cm<sup>-1</sup>.

Figure 6a shows the X-loading plot of the first latent variable (LV1) for the full-spectrum model, highlighting wavenumbers that contribute significantly to model performance. Notable peaks were observed at 4196, 4451, 4528 [N-H (3v)], 5060 (water), 5292, 6791, and 7050 cm<sup>-1</sup>, where the X-loading of 1st latent variable Selected

| Variable selection method | Pretreatment | Wavenumber | Factor | Calibration set |         |                            | Prediction set |         |                            |                           |     |
|---------------------------|--------------|------------|--------|-----------------|---------|----------------------------|----------------|---------|----------------------------|---------------------------|-----|
|                           |              |            |        | N               | $R^2_C$ | RMSEC (J g <sup>-1</sup> ) | n              | $R^2_p$ | RMSEP (J g <sup>-1</sup> ) | Bias (J g <sup>-1</sup> ) | RPD |
| Full wavelength           | Raw          | 1150       | 10     | 147             | 0.94    | 200.35                     | 50             | 0.81    | 386.38                     | 53.99                     | 2.3 |
|                           | SNV          | 1150       | 8      | 147             | 0.95    | 173.26                     | 50             | 0.82    | 373.07                     | 23.18                     | 2.4 |
|                           | FstDev       | 1150       | 9      | 147             | 0.98    | 94.02                      | 50             | 0.85    | 334.48                     | 77.90                     | 2.6 |
|                           | SecDev       | 1150       | 9      | 147             | 0.97    | 31.94                      | 50             | 0.58    | 578.46                     | -64.75                    | 1.5 |
| CM                        | Raw          | 440        | 10     | 147             | 0.94    | 203.35                     | 50             | 0.81    | 386.38                     | 53.99                     | 2.3 |
|                           | SNV          | 205        | 8      | 147             | 0.95    | 174.26                     | 50             | 0.82    | 375.07                     | 23.18                     | 2.4 |
|                           | FstDev       | 490        | 9      | 147             | 0.98    | 94.02                      | 50             | 0.85    | 331.48                     | 77.90                     | 2.6 |
|                           | SecDev       | 365        | 9      | 147             | 0.97    | 31.94                      | 50             | 0.58    | 577.46                     | -64.75                    | 1.5 |
| VM                        | Raw          | 800        | 10     | 147             | 0.94    | 201.35                     | 50             | 0.81    | 387.38                     | 53.99                     | 2.3 |
|                           | SNV          | 1130       | 8      | 147             | 0.96    | 173.26                     | 50             | 0.82    | 374.07                     | 23.18                     | 2.4 |
|                           | FstDev       | 325        | 9      | 147             | 0.98    | 93.02                      | 50             | 0.85    | 333.48                     | 77.90                     | 2.6 |
|                           | SecDev       | 195        | 9      | 147             | 0.98    | 31.94                      | 50             | 0.58    | 576.41                     | -64.75                    | 1.5 |
| COVM                      | Raw          | 790        | 10     | 147             | 0.94    | 200.35                     | 50             | 0.81    | 386.38                     | 53.99                     | 1.7 |
|                           | SNV          | 1130       | 8      | 147             | 0.96    | 173.26                     | 50             | 0.83    | 375.07                     | 23.18                     | 1.7 |
|                           | FstDev       | 360        | 9      | 147             | 0.94    | 201.23                     | 50             | 0.85    | 343.52                     | 56.55                     | 1.8 |
|                           | SecDev       | 365        | 9      | 147             | 0.98    | 92.02                      | 50             | 0.86    | 332.48                     | 77.90                     | 2.7 |
| VIP                       | Raw          | 205        | 10     | 147             | 0.91    | 261.22                     | 50             | 0.75    | 446.09                     | -27.75                    | 2.0 |
|                           | SNV          | 315        | 8      | 147             | 0.91    | 250.93                     | 50             | 0.78    | 441.35                     | 10.83                     | 2.2 |
|                           | FstDev       | 535        | 9      | 147             | 0.94    | 201.63                     | 50             | 0.85    | 344.56                     | 57.68                     | 2.6 |
|                           | SecDev       | 280        | 9      | 147             | 0.98    | 119.18                     | 50             | 0.74    | 451.07                     | 24.60                     | 2.0 |

**Table 5.** Result of HHV prediction by PLSR using different preprocessing spectra and different variable selected methods. N: Number of samples in calibration set,  $R^2_C$ : coefficient of determination of calibration set, n: number of samples in prediction set,  $R^2_p$ : coefficient of determination of prediction set, RPD: ratio of prediction to deviation, CM: correlation method, VM: variance method, COVM: co-variance method, VIP: variable importance of projection, FstDev: 1st derivative, SecDev: 2nd derivative. Significant values are in [bold].



**Fig. 4.** HHV measured by bomb calorimeter versus predicted value by NIR spectroscopy. The optimal model for predicting the HHV of biomass was developed using the 2nd derivative spectra combined with wavenumber selection via the correlation method. This approach reduced the number of variables from 1150 to 365 wavelengths, significantly improving model performance ( $R^2_C=0.98$ ,  $R^2_P=0.86$ ).

wavenumber-loading plot for the selected wavenumber model (Fig. 6b) shows influential peaks at 4065 [ $\text{CH}_3$  (3 $\delta$ )], 4304 [C-H (1v) +  $\text{CH}_2$  (1 $\delta$ )], 4397 (glucose), 4682, 5230 (phosphate), 5307, 6970, 7436, and 8647  $\text{cm}^{-1}$ .

The vibration of most molecular bonds which had strong contribution in prediction of GWP, were in hydrocarbons including cellulose; glucose; water; and protein, even GWP is a functional properties not a constituent in the biomass.

#### Regression coefficient and x-loading of HHV model

Prominent peaks were identified and the bond vibration interpretation is shown in Table 7 and the vibration indicated by Workman and Weyer<sup>38</sup> at the wavenumbers in bold were not found or not related to biomass.

For the HHV prediction model, the regression coefficient plots are presented in Fig. 7. In the full-spectrum model (Fig. 7a), prominent peaks were observed at 4397 (glucose), 4960 [C-H (1v) + O-H (1 $\delta$ )], 5168 (water), 5330, 5947 [C-H (2v)], 6672, and 7506  $\text{cm}^{-1}$ . In contrast, the selected wavenumber model (Fig. 7b) exhibited dominant peaks at 4111 [C-H (1v) + C-H (1 $\delta$ )], 4520 [N-H (3v)], 4644 [C-H (1v) + C-C (1v)], 5307, 5369, 5978 [C-H (1v) + C-H (1v)], 6063, 7020, and 7220  $\text{cm}^{-1}$ .

The LV1 of X-loading plots, shown in Fig. 8, highlights the critical wavenumbers contributing to the model's performance. In the full-spectrum model (Fig. 8a), significant peaks were found at 4165 [C-H (1v) + C-H (1 $\delta$ )], 4435, 4520, 5037, 5292, 6595, and 7112 [O-H (2v)]  $\text{cm}^{-1}$ . The selected wavenumber model (Fig. 8b) revealed key peaks at 4034, 4134 [C-H (1v) + C-H (1 $\delta$ )], 4443, 4983, 5230 (phosphate), 5361, 5963 [C-H (2v)], 7081 and 7274  $\text{cm}^{-1}$ .

The similar bond vibration contributed to prediction of both HHV and GWP including 5230 (phosphate), (5168 and 5214 nm, respectively) water, (4651, 4644 nm, respectively) [C-H (1v) + C-C (1v)], (4520, 4528 nm, respectively) [N-H (3v)], 4397 (glucose), and (4134, 4142 nm, respectively) [C-H (1v) + C-H (1 $\delta$ )], obviously.

#### Averaging reference value of GWP and HHV parameter of biomass

GWP and HHV are essential for optimizing biomass as a renewable energy source and mitigating its environmental impact. The environmental sustainability of biomass is primarily assessed using the GWP measured in  $\text{CO}_2$  equivalents over a 100-year period.

Table 6 illustrates the average reference value of GWP and HHV ( $\text{J g}^{-1}$ ) of fast-growing trees and agricultural residues. It shows that the fast-growing trees possess variability in their values reflect slight variations in their chemical composition and energy content, influencing the different biomass applications. They underline the variability within agricultural residues, impacting their efficiency and environmental impact when used as bioenergy sources. It shows that fast-growing trees generally possess higher heating values and carbon content, making them more efficient as biomass fuels. However, the GWP values indicate varying degrees of environmental impact, which is crucial for sustainable energy production. Most of agricultural residues, while slightly lower in energy content, offer a viable alternative due to their abundance and ease of collection with

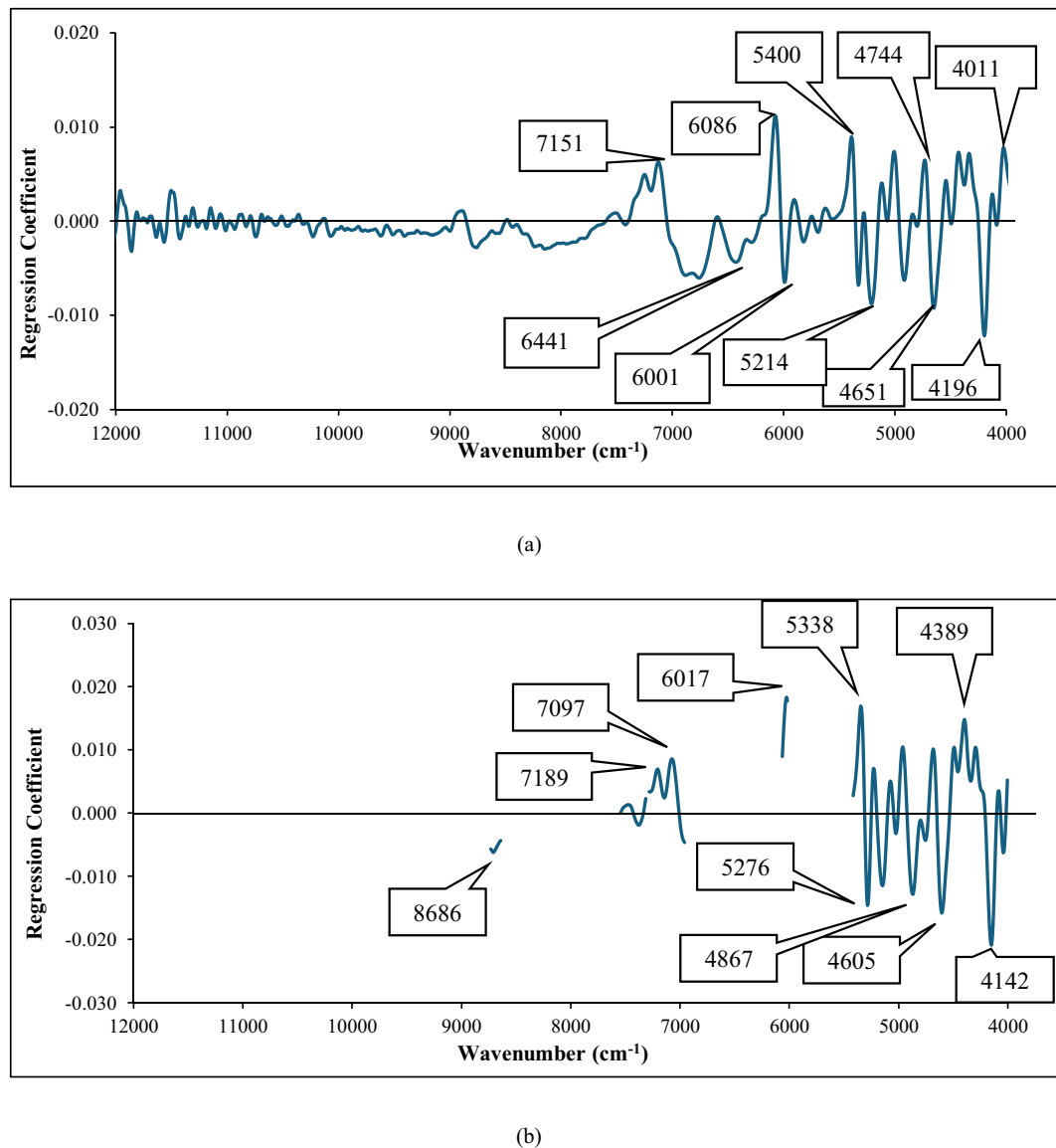


**Fig. 5.** Regression coefficient of GWP calibration model using 1st derivative spectra with full wavenumbers (a) and selected wavenumber (b). The peaks in the regression coefficient plot highlight molecular bond vibrations, where high positive and high negative peaks indicate the vibration of the wavenumber is significantly high influence the prediction values.

their lower GWP values necessitate careful consideration in their use to mitigate climate impact. These insights into the chemical and energy profiles of various biomass resources provide a foundation for selecting optimal materials for bioenergy, balancing efficiency, and environmental sustainability (Table 7).

The scatter plot illustrates the correlation between GWP and HHV across three distinct sample groups: fast-growing trees (Fig. 9a), agricultural residues (Fig. 9b), and a mixture of fast-growing trees and agricultural residues (Fig. 9c). The results indicate a strong linear relationship between GWP and HHV, with a coefficient of determination ( $R^2$ ) equal to 1, demonstrating perfect fit. The equation governing the calculation of GWP from HHV is consistent across all sample types and is expressed as  $\text{GWP or GWP total} = 2098.0 \times \text{HHV in TJ kg}^{-1} = 0.000002098 \times \text{HHV in kJ kg}^{-1} = 0.000002098 \times \text{HHV in Jg}^{-1}$ .

However, the HHV direct measurement is destructive, time consuming and chemical is necessary, therefore, it is not environmentally friendly. But our NIRS proposed method in this report is non-destructive, fast and no chemical is necessary, therefore, environmentally friendly.

It can be perfect fit based on the IPCC guideline recommendation, the GHG emission in our calculation is for 1 kg biomass sample (It can be perfect fit even if the different number is used but it have to be fixed throughout the calculation).

The calculation for proving the perfect fit between GWP and HHV is shown in following

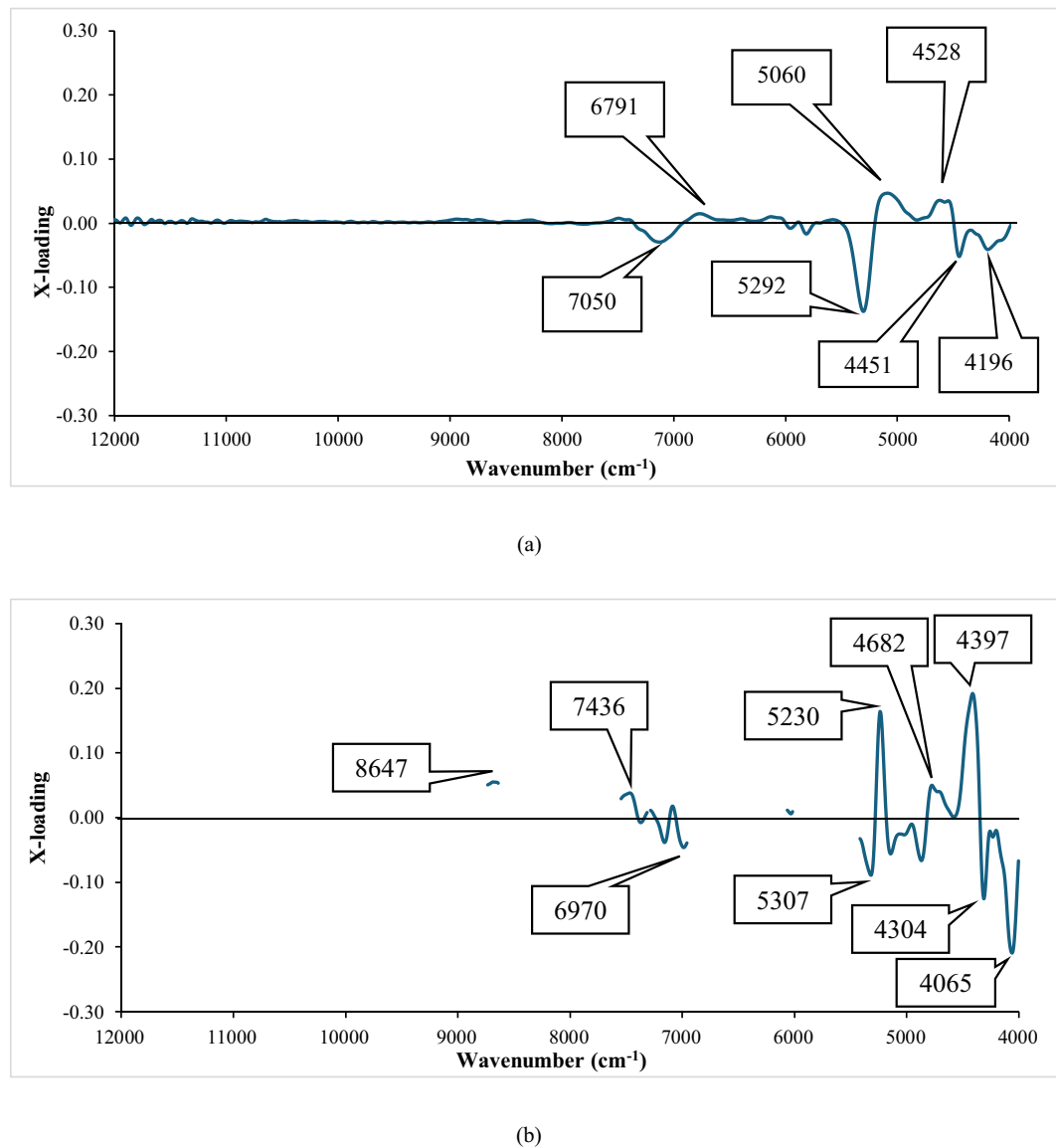


**Fig. 6.** X-loading plot of latent variable 1 of GWP model developed using 1st derivative spectra with full wavenumber range (a) and selected wavenumber (b). The peaks in the X-loading plot highlight molecular bond vibrations, where high positive and high negative peaks indicate the vibration of the wavenumber is significantly high influence the latent variable score values.

$$\begin{aligned}
 & \text{GHG (e.g. CO}_2\text{, or CH}_4\text{, or N}_2\text{O) Emissions (kg)} \\
 & = \text{Mass of biomass sample (kg)} \times \text{HHV of biomass sample (TJ kg}^{-1}\text{)} \\
 & \quad \times \text{Emission Factor (EF) of corresponding GHG (kg TJ}^{-1}\text{)}
 \end{aligned} \tag{7}$$

GHG Emissions (kg) represents the total amount of emissions produced. Mass of biomass samples (kg) refers to the total mass of the biomass sample burnt. High heating value (HHV) ( $\text{TJ kg}^{-1}$ ) is the total amount of energy in TJ obtained by 1 kg of biomass completely burnt in bomb calorimeter. According to the IPCC 2021 Guidelines, default greenhouse gas emission factors (in  $\text{kg TJ}^{-1}$ ) for wood and woody biomass combustion are 112  $\text{kg CO}_2/\text{TJ}$  (non-biogenic  $\text{CO}_2$  only), 30  $\text{kg CH}_4/\text{TJ}$ , and 4  $\text{kg N}_2\text{O/TJ}$ , expressed based on energy content of the fuel burned<sup>7</sup>.

Substitute the constant numbers and solely the HHV is variable which multiplied with constant number provided simple linear equation and the constant number is slope of the equation

GHG (e.g.  $\text{CO}_2$ , or  $\text{CH}_4$ , or  $\text{N}_2\text{O}$ ) Emissions (kg) = 1 (kg)  $\times$  HHV of biomass sample ( $\text{TJ kg}^{-1}$ )  $\times$  112  $\text{kg CO}_2/\text{TJ}$  (non-biogenic  $\text{CO}_2$  only) or 30  $\text{kg CH}_4/\text{TJ}$ , or 4  $\text{kg N}_2\text{O/TJ}$ , respectively, used for Emission Factor (EF) of corresponding GHG ( $\text{kg TJ}^{-1}$ )

$\text{CO}_2$ , or  $\text{CH}_4$ , or  $\text{N}_2\text{O}$  Emissions (kg) = 112  $\times$  HHV, 30  $\times$  HHV and 4  $\times$  HHV for  $\text{CO}_2$ , or  $\text{CH}_4$ , or  $\text{N}_2\text{O}$  Emissions, respectively

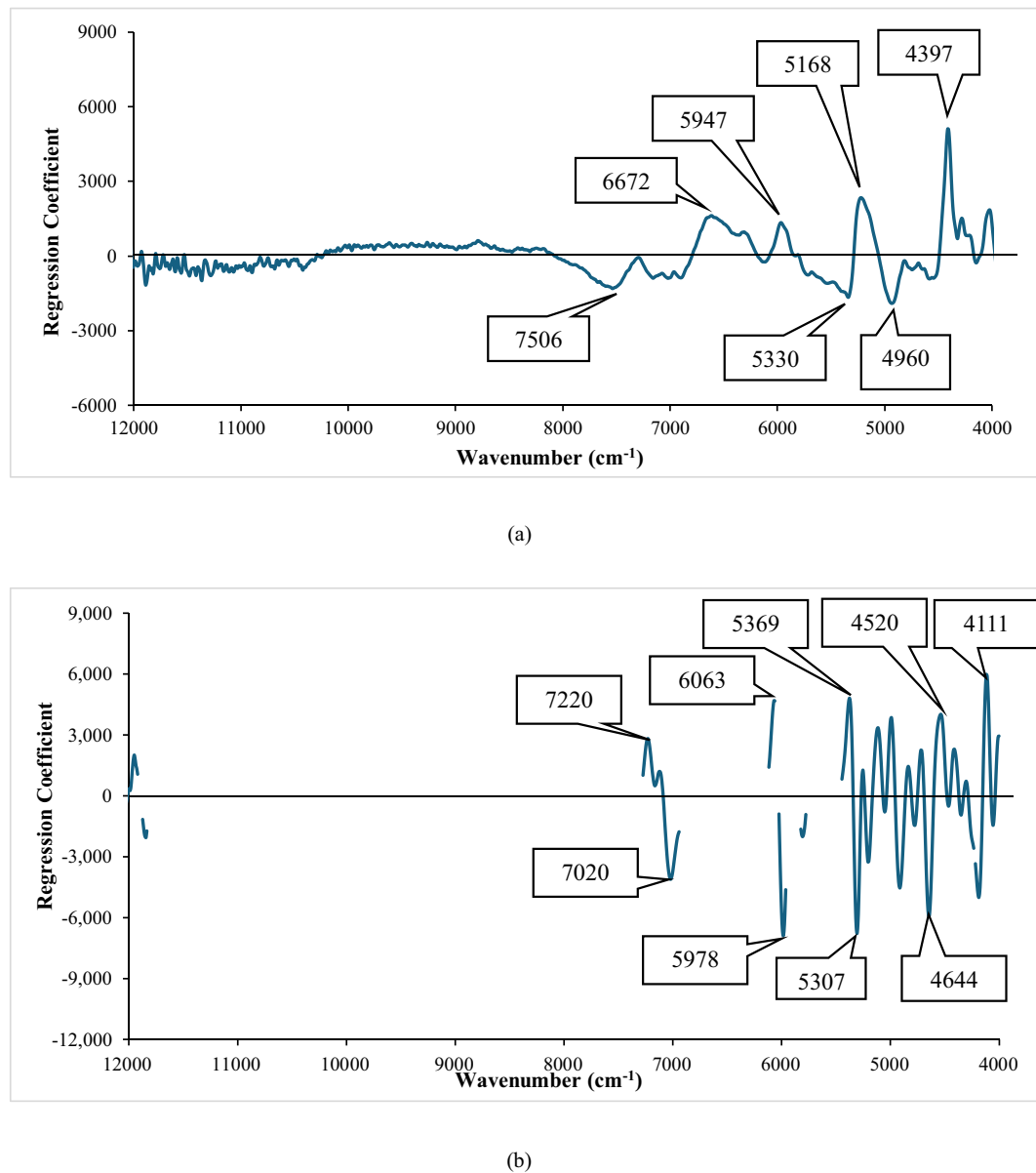


**Fig. 7.** Regression coefficient of HHV calibration model using 1st derivative spectra with full wavenumbers (a) and selected wavenumber (b). The peaks in the regression coefficient plot highlight molecular bond vibrations, where high positive and high negative peaks indicate the vibration of the wavenumber is significantly high influence the prediction values.

Using the Global Warming Potential (GWP) values recommended by IPCC (2021) 6th Assessment Reports (AR6)<sup>7</sup>, 1 by CO<sub>2</sub>, 29.8 by CH<sub>4</sub>, and 273 by N<sub>2</sub>O, the total GWP was computed for 100 year based as:

Substitute the constant numbers and solely the HHV is variable which multiplied with constant number provided simple linear equation and the constant number is slope of the equation

$$\begin{aligned}
 \text{GWP for CO}_2, \text{ or CH}_4, \text{ or N}_2\text{O Emissions} &= (1 \times \text{CO}_2 \text{ Emission}) \\
 &\text{or } (29.8 \times \text{CH}_4 \text{ Emission}) \text{ or } (273 \times \text{N}_2\text{O Emission}) \\
 &= (1 \times 112 \text{ HHV}) \text{ for CO}_2 \text{ Emission or } (29.8 \times 30 \text{ HHV}) \\
 &\text{for CH}_4 \text{ Emission or } (273 \times 4 \text{ HHV}) \text{ for N}_2\text{O Emission} \\
 &= 112.0 \times \text{HHV for CO}_2 \text{ Emission or } 894.0 \times \text{HHV} \\
 &\text{for CH}_4 \text{ Emission or } 1092.0 \times \text{HHV for N}_2\text{O Emission} \\
 \text{and GWP total} &= 2098.0 \left( \text{HHV, } \text{TJ kg}^{-1} \right) \\
 &= 0.000002098 \text{ kJ kg}^{-1} = 0.000002098 \text{ Jg}^{-1}
 \end{aligned} \tag{8}$$

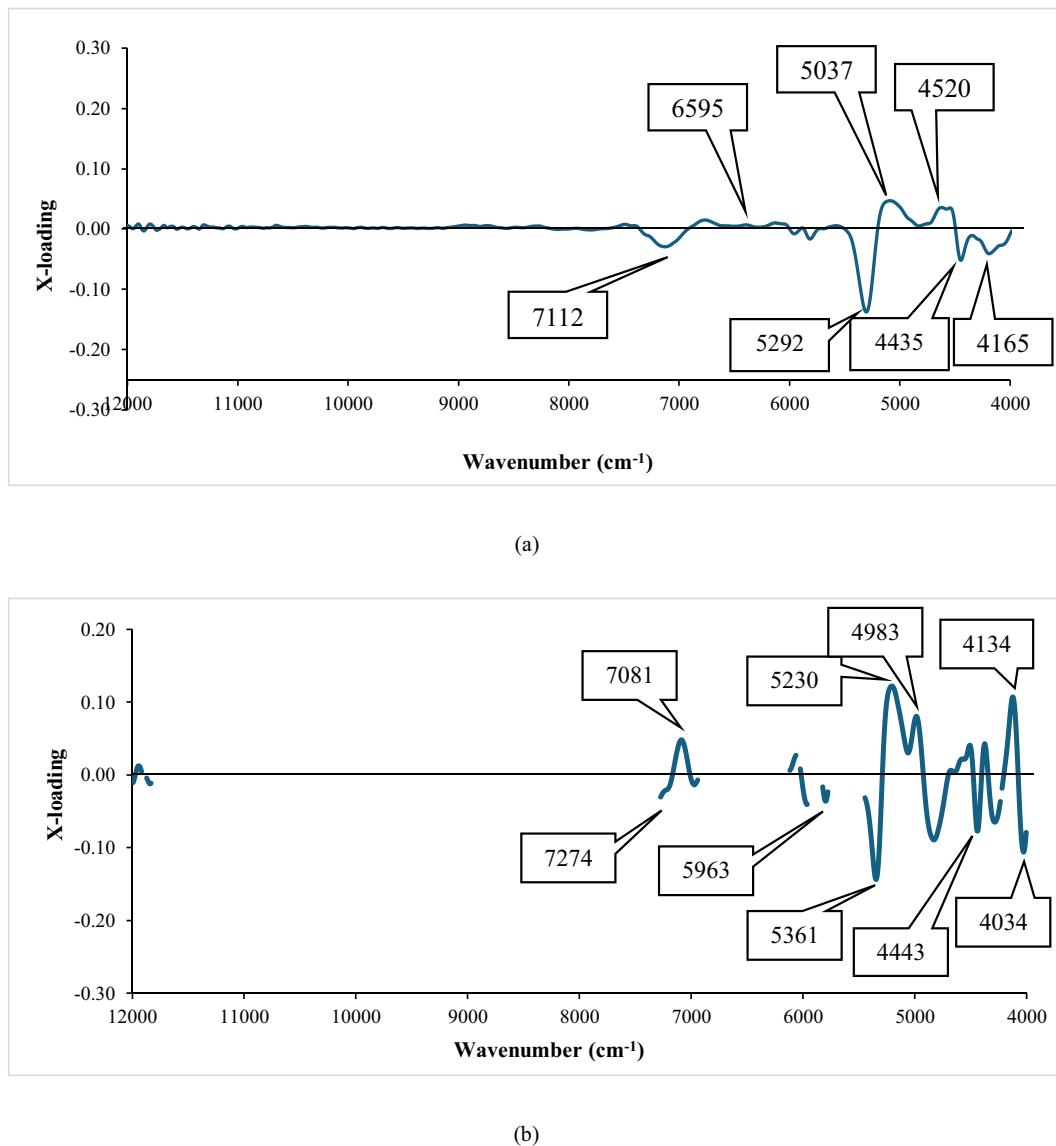


**Fig. 8.** X-loading plot of HHV model developed by using 2nd derivative spectra with full wavenumbers (a) and selected wavenumber (b). The peaks in the regression coefficient plot highlight molecular bond vibrations, where high positive and high negative peaks indicate the vibration of the wavenumber is significantly high influence the prediction values.

| Category             | Name of Species                 | $\text{CO}_2$ Emission (kg) | GWP mean value ( $\pm \text{SD}$ ) | HHV ( $\text{J g}^{-1}$ ) |
|----------------------|---------------------------------|-----------------------------|------------------------------------|---------------------------|
| fast-growing tree    | <i>Alnus nepalensis</i>         | $2.05 \times 10^{-3}$       | $0.0364 \pm 0.0010$                | 17,932                    |
|                      | <i>Pinus roxburghii</i>         | $2.00 \times 10^{-3}$       | $0.0416 \pm 0.0009$                | 18,349                    |
|                      | <i>Bombusa vulagris</i>         | $1.93 \times 10^{-3}$       | $0.0367 \pm 0.0012$                | 17,310                    |
|                      | <i>Eucalyptus Camaldulensis</i> | $1.91 \times 10^{-3}$       | $0.0372 \pm 0.0009$                | 17,105                    |
|                      | <i>Bombax Ceiba</i>             | $1.91 \times 10^{-3}$       | $0.0375 \pm 0.0007$                | 17,077                    |
| agricultural residue | <i>Zea mays(cob)</i>            | $1.93 \times 10^{-3}$       | $0.0379 \pm 0.0007$                | 17,297                    |
|                      | <i>Zea mays(shell)</i>          | $1.90 \times 10^{-3}$       | $0.0375 \pm 0.0011$                | 16,409                    |
|                      | <i>Zea mays (stover)</i>        | $1.87 \times 10^{-3}$       | $0.0367 \pm 0.0003$                | 16,753                    |
|                      | <i>Oryza sativa</i>             | $1.83 \times 10^{-3}$       | $0.0347 \pm 0.0006$                | 15,417                    |
|                      | <i>Saccharum officinarum</i>    | $1.72 \times 10^{-3}$       | $0.0376 \pm 0.0004$                | 17,029                    |

**Table 6.** Average of reference value of GWP and HHV ( $\text{J g}^{-1}$ ) of fast-growing trees and agricultural residues.

| Wavenumber (cm <sup>-1</sup> ) | Wavenumber (cm <sup>-1</sup> ) indicated in <sup>38</sup> | Bond vibration                              | Structure        | Model  |
|--------------------------------|---|---|------------------|--|
| 4011                           | 4019  | C-H (1v) + C-C (1v)                         | Cellulose        | GWP Regression Coefficient Fullwave                      |
| 4065                           | 4068  | CH <sub>3</sub> (3δ)                        | Hydrocarbons     | GWP X-loading of 1st latent variable Selected wavenumber |
| 4111, 4134, 4142, 4165, 4196   | 4190-4090   | C-H (1v) + C-H (1δ)                         | C-H Aryl         | GWP Regression Coefficient Fullwave                      |
|                                |   |   |                  | GWP Regression Coefficient Selected wavenumber           |
|                                |   |   |                  | GWP X-loading of 1st latent variable Fullwave            |
|                                |   |   |                  | HHV Regression Coefficient Selected wavenumber           |
|                                |   |   |                  | HHV X-loading of 1st latent variable Fullwave            |
|                                |   |   |                  | HHV X-loading of 1st latent variable Selected wavenumber |
| 4304                           | 4307  | C-H (1v) + CH <sub>2</sub> (1δ)             | Glucose          | GWP X-loading of 1st latent variable Selected wavenumber |
| 4389                           | 4386  | C-H (1v) + CH <sub>2</sub> (1δ)             | Polysaccharides  | GWP Regression Coefficient Selected wavenumber           |
| 4397                           | 4400  | O-H (1v) + C-O (1v)                         | Glucose          | GWP X-loading of 1st latent variable Selected wavenumber |
|                                |   |   |                  | HHV Regression Coefficient Fullwave model                |
| 4520, 4528                     | 4525  | N-H (3v)                                    | Ammonia in water | GWP X-loading of 1st latent variable Fullwave            |
|                                |   |   |                  | HHV Regression Coefficient Selected wavenumber           |
|                                |   |   |                  | HHV X-loading of 1st latent variable Fullwave            |
| 4605                           | 4600  | CONH <sub>2</sub>                           | Proteins         | GWP Regression Coefficient Selected wavenumber           |
| 4644, 4651                     | 4644  | C-H (1v) + C-C (1v)                         | C-H Aryl         | GWP Regression Coefficient Fullwave                      |
|                                |   |   |                  | HHV Regression Coefficient Selected wavenumber           |
| 4867                           | 4866  | N-H (1v) + C=O (1v) (amide I)               | Amides/proteins  | GWP Regression Coefficient Selected wavenumber           |
| 4960                           | 4960  | O-H (1v) + O-H (1δ)                         | Methanol O-H     | HHV Regression Coefficient Fullwave                      |
| 5060                           | 5049  | N-H (1v) + N-H (1δ)                         | Aromatic amine   | GWP X-loading of 1st latent variable Fullwave            |
| 5168                           | 5160  | O-H — v2 + v3                               | water            | HHV Regression Coefficient Fullwave                      |
| 5214                           | 5200  | O-H (1v) + O-H (1δ)                         | water            | GWP Regression Coefficient Fullwave                      |
| 5230                           | 5241  | P-OH — O-H (2v)                             | Phosphate        | GWP X-loading of 1st latent variable Selected wavenumber |
|                                |   |   |                  | HHV X-loading of 1st latent variable Selected wavenumber |
| 5947, 5963                     | 5952  | C-H (2v)                                    | Hydrocarbons     | HHV Regression Coefficient Fullwave                      |
|                                |   |   |                  | HHV X-loading of 1st latent variable Selected wavenumber |
| 5978                           | 5985  | C-H (1v) + C-H (1v)                         | C-H Aryl         | HHV Regression Coefficient Selected wavenumber           |
| 6441                           | 6450  | O-H   | water            | GWP Regression Coefficient Fullwave                      |
| 7112                           | 7100  | O-H (2v)                                    | O-H (Methanol)   | HHV X-loading of 1st latent variable Fullwave            |
| 7151                           | 7163  | CH <sub>3</sub> (2v) + CH <sub>3</sub> (1δ) | Hydrocarbons     | GWP Regression Coefficient Fullwave                      |
| 7189                           | 7194  | CH <sub>3</sub> (2v) + CH <sub>3</sub> (1δ) | Hydrocarbons     | GWP Regression Coefficient Selected wavenumber           |

**Table 7.** The function groups corresponding to wavenumber shown in regression coefficient plot and x-loading plot of models for GWP and HHV. \*1v, fundamental stretching vibration; 2v, 1st overtone of fundamental stretching vibration; 3v, 2nd overtone of fundamental stretching vibration; 5v, 4th overtone of fundamental stretching vibration; 1δ, fundamental bending (deformation) vibration; 3δ, 2nd overtone of fundamental bending (deformation) vibration; 1, symmetric stretching vibration; 2, bending vibration; 3, asymmetric stretching vibration; and + is combination.

## Discussion

The prediction of GWP of biomass using FT-NIR spectroscopy presents an innovative approach to evaluating the environmental impact of biomass energy sources. Biomass is increasingly considered a vital renewable energy resource, but its sustainability is contingent upon a comprehensive understanding of its environmental implications, particularly its GWP, which reflects its contribution to climate change.

## Correlation between HHV and GWP

The results exhibit a correlation between the chemical composition of biomass within its FT-NIR spectrum, and its GWP. The FT-NIR technique scanned the vibrational signatures of molecular bonds in the biomass, which reveal its composition, particularly in terms of cellulose, hemicellulose, lignin, and moisture content<sup>45</sup>. These compositional factors directly influence the biomass's HHV and, consequently, its GWP. The positive correlation examined in the study between HHV and GWP suggests that biomass with a higher energy content tends to have a higher GWP, likely due to the increased carbon content, which results in greater CO<sub>2</sub> emissions upon combustion. NIR spectroscopy can be used to assess biomass's carbon content, which is directly connected to the amount of CO<sub>2</sub> it emits when burned<sup>46</sup>. Building on this, our work incorporates emissions of CH<sub>4</sub> and N<sub>2</sub>O in addition to CO<sub>2</sub> and establishes a direct correlation between GWP and the NIR spectral data.

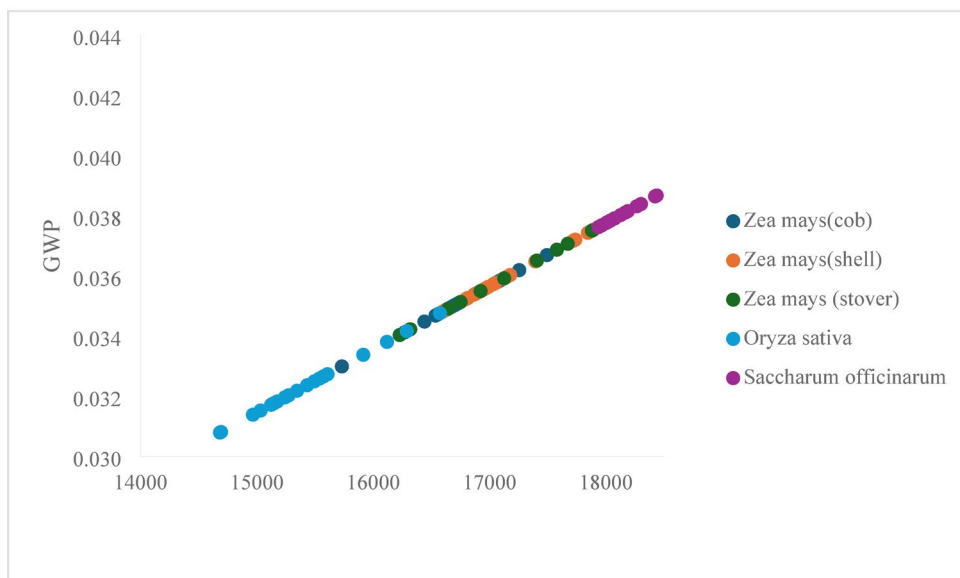
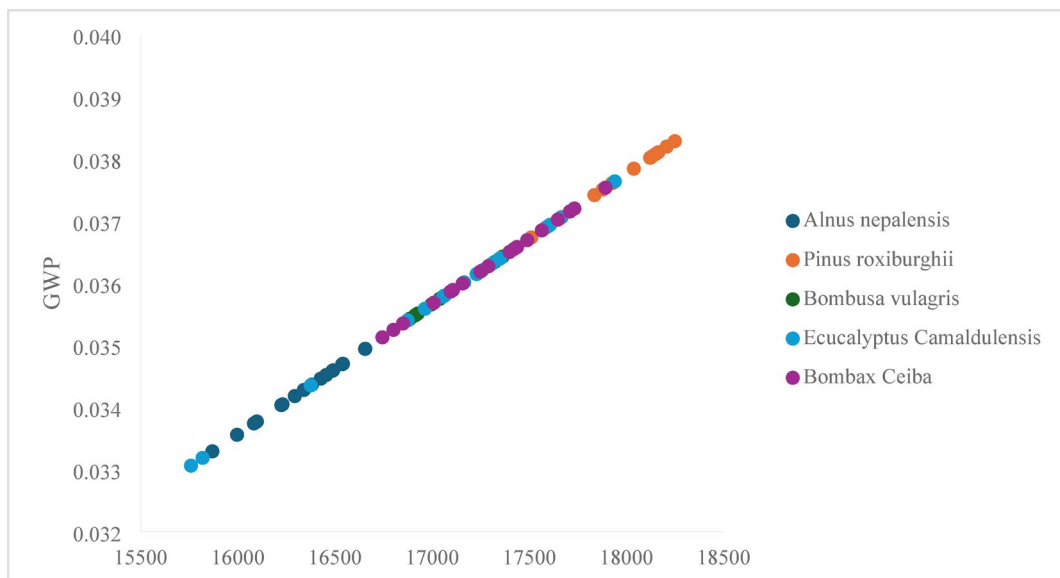
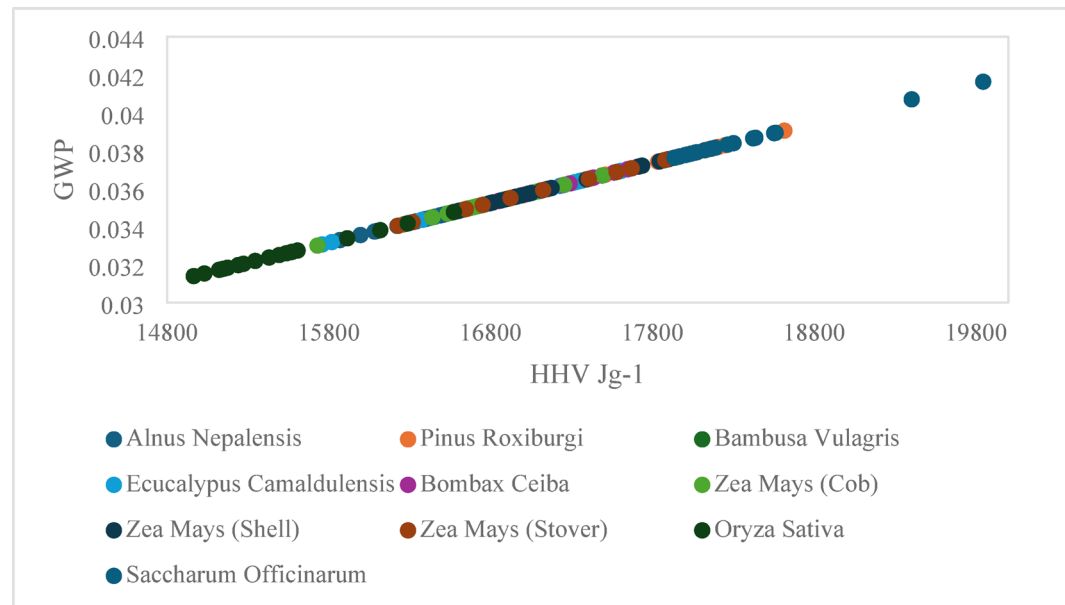


**Fig. 9.** Scatter plots of GWP value with different HHV of every sample of fast-growing trees (a), every sample of agriculture residues (b) and every sample of fast-growing trees and agriculture residue (c). The scatter plot with a trend line, illustrating the relationship between Higher Heating Value (HHV) and Global Warming Potential (GWP) for fast-growing trees and agricultural residue biomass. The plot shows a positive correlation, indicating that biomass with higher HHV tends to contribute more to GWP. Data points are color-coded by biomass type and mostly fall within the mid-range of HHV (15,800–18,000 J g<sup>-1</sup>) and GWP (0.0320–0.0380). This suggests that higher energy content in biomass is associated with greater environmental impact due to increased emissions.

#### Prediction model and its accuracy

The predictive models shown in Fig. 3 used FT-NIR data and modeling technique of PLSR exhibit for the acceptable accuracy in estimating the GWP of various biomass types. The  $R_p^2$  values of 0.85 indicated optimized 325 wavenumber found by COVM with 1st derivative spectra in our study provided the model with a substantial proportion of the variance in GWP can be explained by the spectral data, affirming the effectiveness of FT-NIR as a non-destructive, rapid, and cost-effective method for GWP estimation. The prediction of GWP in real-time can substantially enhance the decision-making process in biomass selection for energy production, ensuring sustainability goals. This is the innovative and unique model to find out the GWP using FT-NIR spectroscopy. The model performance of HHV is shown in Fig. 4, where the  $R_p^2$  values is 0.86 by 2nd derivative spectra of optimized 365 wavenumbers found by COVM.



c full raw data of biomass of fast-growing trees and agriculture residue

**Fig. 9.** (continued)

Williams et al.<sup>37</sup> have developed a guideline for model performance interpretation based on  $R^2_p$  value and RPD value, where, our case,  $R^2_p$  of 0.85 for GWP and 0.86 for HHV is in the range of 0.83–0.90 is usable with caution for most applications including research and RPD of 2.6 for GWP and 2.7 for HHV are in the range of 2.5–2.9 for functionality parameter such as GWP and HHV indicating the models are fair and can be used for screening. We therefore, interpret our GWP and HHV optimized models can be usable with caution for most applications including research based on its  $R^2_p$ .

The developed PLSR model is built on a mixture of five fast-growing tree species and five types of agricultural residues, which is same biomass data set as Shrestha et al.<sup>18</sup> who reported the effect of diffent species to model performance for prediction of C, H, N, and O content in biomass. The result shows for C model to be better the pine and corn stover should not be include in modeling, for N model, pine, and bagasse should not be included, for H, pine, Alnus, corn shell, and bagasse should not be included; and for O, pine should not be included for better performance of the models<sup>18</sup>. This indicated pine was not be included in any model of these groups of biomass with the rational by Williams principle<sup>37</sup> to be explained.

Williams et al.<sup>37</sup> explained that the rate of change of Y (measured value) is a function of the rate of change of X (NIR predicted value) can be indicated by slope of the trend line plotted between Y and X<sup>18,37</sup>, when the R approached 1 and the slope approached 1 and the intercept approached zero, the model approached excellence<sup>37</sup>. This is the dictation principal to remove or keep the species which have negative and positive effect, respectively, on the model performance. The combined different species of biomass, for example, in our case, the fast-growing trees and agricultural residue, Shrestha et al.<sup>18</sup> indicated the inclusion of different species in a model, the species have to be not only in the different values of the constituents to make a wider range for a robust model, but every specie also must provide the characteristic of the same rate of change of NIR predicted values with the measured values (same slope and slope should approach 1, and intercept is same (no gap) and approached zero), for high performance of prediction. Some species whose characteristics were similar, the trends were common supported the each other but might positively or negatively to the prediction performace of the model<sup>18</sup>. By scatter plot (trend line) analysis, which of the species affecting the model negatively were identified and dictated how to improve the model performance<sup>18</sup>.

The H content contributed more on HHV compared to C content<sup>47,48</sup>. Higher concentrations of O and moisture ( $H_2O$ ), in turn, lower the HHV, resulting in incomplete combustion<sup>48</sup>. High C and H but low in N, S, and  $H_2O$  is the besttype of biomass maximizing the amount of energy i.e. HHV<sup>48</sup>. These element in biomass highly related to GHG emissions<sup>48</sup>, therefore, GWP. The further study and investigation of these relations can bring some conclusions of Global warming management effectively.

#### Analysis of traditional method and FT-NIR spectroscopy

The traditional methods of GWP estimation, which often involve complex chemical analyses and life cycle assessment (LCA) models whereas FT-NIR spectroscopy approaches a more streamlined. Traditional methods, while comprehensive, can be time-consuming and resource intensive. FT-NIR, by contrast, provides rapid results, making it an attractive tool for routine analysis and large-scale biomass screening<sup>39</sup>.

Though, FT-NIR offers rapid, non-destructive, and cost-effective GWP prediction, it has certain limitations. For instance, the developed model's accuracy will be affected by other variability in biomass composition, such

as differences in moisture content, lignin, or cellulose levels, if were not included in the model. The updating model can be optimized by include more varieties and species of biomass to obtain more robust prediction performance. However, it is essential to note that while FT-NIR can predict GWP based on biomass composition, it does not account for the entire lifecycle emissions, such as those from cultivation, harvesting, transportation or processing. While FT-NIR is highly effective for rapid screening, it should be used in conjunction with other LCA tools for a holistic assessment.

### Sustainable approach to implications for biomass energy sector

The ability to predict GWP using FT-NIR spectroscopy has significant implications for the biomass energy sector. By enabling more precise selection of biomass feedstocks with lower GWP, this approach supports the development of more sustainable bioenergy systems. This could lead to a reduction in the overall carbon footprint of bioenergy production, making it a more competitive alternative to fossil fuels in the context of global climate change mitigation<sup>49</sup>.

### Future research and way forward

Future research should focus on expanding the database of biomass types analyzed using FT-NIR to improve the robustness and generalizability of the predictive models. Additionally, integrating FT-NIR data with thermogravimetric analysis (TGA) where the simulation of different type thermal conversion of biomass degrading in which the different emission gases are generated and with gas chromatography-mass spectrometry (GC-MS) for evaluation of concentration of the generated emission gases could further refine GWP predictions by providing more comprehensive insights and exact content of emission gases effect global warming to support the IPCC. Moreover, exploring the use of FT-NIR in conjunction with different machine learning algorithms could enhance the predictive power of the models, allowing for more accurate GWP estimation across a broader range of biomass types.

### Conclusion

In this research, PLSR-based model developed and compared using FT-NIR spectroscopy to analyze the global warming potential (GWP) of fast-growing trees and agricultural residue biomass. All chip biomass samples were scanned within 3600–12,500 cm<sup>-1</sup> on the diffuse reflectance with macro sphere sample rotating mode, with a particular emphasis on their suitability for energy applications. The prediction model was developed using the full standard normal variate (SNV) or featured wavenumbers obtained by Correlation Matrix (CM), Variance Matrix (VM), Covariance Matrix (COVM) and Variable Importance of Projection (VIP) coupled with four pretreatment methods including raw spectra, 1st Derivative, 2nd Derivative, and standard normal variate (SNV). The model with the optimum performance was selected based on trade-off parameters of  $R^2_C$ , RMSEC,  $R^2_P$ , RMSEP, RPD and bias.

This research lays a foundation in NIRS, showing that preprocessing on the full wavenumber range spectra with various techniques can enhance model accuracy. The recommended PLSR models for rapid assessing GWP by biomass combustion developed by 1st derivative pretreated spectra with selected wavenumber obtained by COVM can serve as a reliable and nondestructive alternative method without of using the measured higher heating value (HHV) value when employing NIRS which only the NIR spectrum of the biomass is needed. It is nondestructive protocol developed for the first time for climate change which usable with caution for most applications including research interpreted followed Williams Guidelines<sup>37</sup>. Therefore, it is necessary to expand sample size from various samples to enhance the model robustness and validate it with unknown samples for proving. We employed the GWP calculation method indicated by IPCC combined with PLSR (Partial Least Squares Regression) modeling achieving a prediction model performance with  $R^2_C=0.92$  and  $R^2_P=0.85$  which demonstrates an optimized model could be used with caution for most application including research. In upcoming paper modeling, we plan to further enhance the model performance by other machine learning techniques such as Random Forest and Support Vector Regression and deep learning such as CNN which may or may not be more accurate in GWP predictions than PLSR in this manuscript.

GWP varies significantly with changes in both HHV and the Emission Factor. This analysis indicates that while both parameters directly influence GWP, the magnitude of their impact can differ depending on specific conditions. For instance, a 10% increase in the Emission Factor could result in a significant rise in GWP, whereas a similar 10% increase in HHV might have a less impact on GWP. This explains that focusing on reducing emissions (e.g. through cleaner combustion technologies or better fuel treatment) could be more effective in reducing overall GWP than merely increasing fuel efficiency.

Furthermore, the research finding could assist academic and research institutions, policymaking think tanks, and energy companies in effective planning, managing, and utilization of bio-resources to meet future energy demands and mitigating the global warming. Additionally, this research outcomes open opportunities for NIR-based research to implement similar approaches.

### Data availability

The datasets generated and/or analysed during the current study are not publicly available due to reasons of no permission of research grant resource but are available from the corresponding author on reasonable request.

Received: 18 December 2024; Accepted: 4 July 2025

Published online: 30 September 2025

## References

1. Holtsmark, B. Quantifying the global warming potential of CO<sub>2</sub> emissions from wood fuels. *Gcb Bioenergy* **7**(2), 195–206 (2015).
2. Zwiers, F. W., Alexander, L. V., Hegerl, G. C., Knutson, T. R., Kossin, J. P., Naveau, P., Nicholls, N., Schär, C., Seneviratne, S. I. & Zhang, X. Climate extremes: challenges in estimating and understanding recent changes in the frequency and intensity of extreme climate and weather events. In *Climate Science for Serving Society: Research, Modeling and Prediction Priorities* 339–389 (2013).
3. Nema, P., Nema, S. & Roy, P. An overview of global climate changing in current scenario and mitigation action. *Renew. Sustain. Energy Rev.* **16**(4), 2329–2336. <https://doi.org/10.1016/j.rser.2012.01.044> (2012).
4. Verbruggen, A. et al. Renewable energy costs, potentials, barriers: Conceptual issues. *Energy Policy* **38**(2), 850–861. <https://doi.org/10.1016/j.enpol.2009.10.036> (2010).
5. Singh, B. R. & Singh, O. Study of impacts of global warming on climate change: rise in sea level and disaster frequency. In *Global Warming—Impacts and Future Perspective* 94–118 (2012).
6. Trenberth, K. E. Attribution of climate variations and trends to human influences and natural variability. *Wiley Interdiscip. Rev. Clim. Change* **2**(6), 925–930 (2011).
7. Intergovernmental Panel on Climate Change Climate change 2021: The physical science basis. In *Contribution of Working Group I to the Sixth Assessment Report of the Intergovernmental Panel on Climate Change* (eds Masson-Delmotte, V. et al. et al.) (Cambridge University Press, 2021).
8. Hickmann, T., Widerberg, O., Lederer, M. & Pattberg, P. The United Nations Framework Convention on Climate Change Secretariat as an orchestrator in global climate policymaking. *Int. Rev. Adm. Sci.* **87**(1), 21–38 (2021).
9. ZangerolameTaroco, L. S. & SabbáColares, A. C. The unframework convention on climate change and the Paris agreement: Challenges of the conference of the parties. *Prolegómenos* **22**(43), 125–135 (2019).
10. Popovski, V. *The Implementation of the Paris Agreement on Climate Change* (Routledge, 2018).
11. Kikstra, J. S. et al. The IPCC Sixth Assessment Report WGI climate assessment of mitigation pathways: from emissions to global temperatures. *Geosci. Model Dev.* **15**(24), 9075–9109 (2022).
12. Carrington, G. & Stephenson, J. The politics of energy scenarios: Are International Energy Agency and other conservative projections hampering the renewable energy transition? *Energy Res. Soc. Sci.* **46**, 103–113 (2018).
13. Bisht, A. S. & Thakur, N. Small scale biomass gasification plants for electricity generation in India: Resources, installation, technical aspects, sustainability criteria & policy. *Renew. Energy Focus* **28**, 112–126 (2019).
14. McKendry, P. Energy production from biomass (part 1): Overview of biomass. *Bioresour. Technol.* **83**(1), 37–46. [https://doi.org/10.1016/S0960-8524\(01\)00118-3](https://doi.org/10.1016/S0960-8524(01)00118-3) (2002).
15. Den, W., Sharma, V. K., Lee, M., Nadadur, G. & Varma, R. S. Lignocellulosic biomass transformations via greener oxidative pretreatment processes: Access to energy and value-added chemicals. *Front. Chem.* **6**, 141 (2018).
16. O'Dea, R. M., Willie, J. A. & Epps, T. H. III. 100th anniversary of macromolecular science viewpoint: Polymers from lignocellulosic biomass. Current challenges and future opportunities. *ACS Macro Lett.* **9**(4), 476–493 (2020).
17. Shrestha, B., Posom, J., Sirisomboon, P. & Shrestha, B. P. Comprehensive assessment of biomass properties for energy usage using near-infrared spectroscopy and spectral multi-preprocessing techniques. *Energies* **16**(14), 5351 (2023).
18. Shrestha, B., Posom, J., Sirisomboon, P., Shrestha, B. P. & Funke, A. Effect of combined non-wood and wood spectra of biomass chips on rapid prediction of ultimate analysis parameters using near infrared spectroscopy. *Energies* **17**(2), 439. <https://doi.org/10.3390/en17020439> (2024).
19. McKendry, P. Energy production from biomass (part 2): Conversion technologies. *Bioresour. Technol.* **83**(1), 47–54 (2002).
20. Tanaka, K., O'Neill, B. C., Rokityanskiy, D., Obersteiner, M. & Tol, R. S. Evaluating global warming potentials with historical temperature. *Clim. Change* **96**, 443–466 (2009).
21. Hao, W. M. & Ward, D. E. Methane production from global biomass burning. *J. Geophys. Res. Atmos.* **98**(D11), 20657–20661 (1993).
22. Sato, I., Listyanto, T., Susanti, A. & Kayo, C. Greenhouse gas emissions reduction potential of biomass power generation in Japan using empty fruit bunch pellets from Indonesia. *Tropics* **34**(1), 11–22 (2025).
23. Sun, G. et al. Influence of oxygen carrier on NO<sub>x</sub> and N<sub>2</sub>O emissions in biomass combustion within fluidized beds. *Process Saf. Environ. Prot.* **193**, 364–373 (2025).
24. De Girolamo, A., Lippolis, V., Nordkvist, E. & Visconti, A. Rapid and non-invasive analysis of deoxynivalenol in durum and common wheat by Fourier-Transform Near Infrared (FT-NIR) spectroscopy. *Food Addit. Contam.* **26**(6), 907–917 (2009).
25. Zhang, K., Zhou, L., Brady, M., Xu, F., Yu, J. & Wang, D. Rapid determination of high heating value and elemental compositions of sorghum biomass using near-infrared spectroscopy. In *Paper presented at the 2015 ASABE Annual International Meeting* (2015).
26. Pitak, L., Sirisomboon, P., Saengprachatanarug, K., Wongpichet, S. & Posom, J. Rapid elemental composition measurement of commercial pellets using line-scan hyperspectral imaging analysis. *Energy* **220**, 119698 (2021).
27. Sirisomboon, C. D., Putthang, R. & Sirisomboon, P. Application of near infrared spectroscopy to detect aflatoxigenic fungal contamination in rice. *Food Control* **33**(1), 207–214 (2013).
28. Posom, J. & Sirisomboon, P. Evaluation of the moisture content of *Jatropha curcas* kernels and the heating value of the oil-extracted residue using near-infrared spectroscopy. *Biosyst. Eng.* **130**, 52–59 (2015).
29. Ortiz Ortega, E., Hosseiniyan, H., Rosales López, M. J., Rodríguez Vera, A. & Hosseini, S. Characterization techniques for chemical and structural analyses. In *Material Characterization Techniques and Applications* 93–152. [https://doi.org/10.1007/978-981-16-9569-8\\_4](https://doi.org/10.1007/978-981-16-9569-8_4) (Springer, 2022).
30. Fearn, T. Standardisation and calibration transfer for near infrared instruments: A review. *J. Near Infrared Spectrosc.* **9**(4), 229–244. <https://doi.org/10.1255/jnirs.309> (2001).
31. Pulles, T., Gillenwater, M. & Radunsky, K. CO<sub>2</sub> emissions from biomass combustion accounting of CO<sub>2</sub> emissions from biomass under the UNFCCC. *Carbon Manag.* **13**(1), 181–189. <https://doi.org/10.1080/17583004.2022.2067456> (2022).
32. Intergovernmental Panel on Climate Change Climate change 2007: The physical science basis. In *Contribution of Working Group I to the Fourth Assessment Report of the Intergovernmental Panel on Climate Change* (eds Solomon, S. et al.) 200–300 (University Press, USA, 2007).
33. Intergovernmental Panel on Climate Change. Climate change 2014: *Synthesis report*. Contribution of Working Groups I, II and III to the Fifth Assessment Report of the Intergovernmental Panel on Climate Change (eds Pachauri, R. K. & Meyer, L. A.). IPCC. <https://www.ipcc.ch/report/ar5/syr/> (2014).
34. Morais, C. L., Santos, M. C., Lima, K. M. & Martin, F. L. Improving data splitting for classification applications in spectrochemical analyses employing a random-mutation Kennard-Stone algorithm approach. *Bioinformatics* **35**(24), 5257–5263 (2019).
35. Barnes, R. J., Dhanoa, M. S. & Lister, S. J. Standard normal variate transformation and de-trending of near-infrared diffuse reflectance spectra. *Appl. Spectrosc.* **43**(5), 772–777. <https://doi.org/10.1366/0003702894202201> (1989).
36. Chong, I. G. & Jun, C. H. Performance of some variable selection methods when multicollinearity is present. *Chemom. Intell. Lab. Syst.* **78**(1–2), 103–112. <https://doi.org/10.1016/j.chemolab.2004.12.011> (2005).
37. Williams, P., Manley, M. & Antoniszyn, J. *Near Infrared Technology: Getting the Best Out of light* (African Sun Media, 2019).
38. Workman, J. Jr. & Weyer, L. *Practical Guide to Interpretive Near-Infrared Spectroscopy* (CRC Press, 2007).
39. Osborne, B. G. *Near Infrared Spectroscopy in Food Analysis*. (Longman Scientific & Technical, New York, 1986).
40. Watt, G. D. A new future for carbohydrate fuel cells. *Renew. Energy* **72**, 99–104. <https://doi.org/10.1016/j.renene.2014.06.025> (2014).

41. U.S. Environmental Protection Agency. Overview of Greenhouse Gases, from <https://www.epa.gov/ghgemissions/overview-green-house-gases> (2024).
42. Apriyanto, A., Compart, J. & Fettke, J. A review of starch, a unique biopolymer—Structure, metabolism and in planta modifications. *Plant Sci.* **318**, 111223. <https://doi.org/10.1016/j.plantsci.2022.111223> (2022).
43. Posom, J., Saechua, W., & Sirisomboon, P. Evaluation of pyrolysis characteristics of milled bamboo using near-infrared spectroscopy. *Renew. Energy* **103**, 653–665 (2017).
44. Posom, J. & Sirisomboon, P. Evaluation of the higher heating value, volatile matter, fixed carbon and ash content of ground bamboo using near infrared spectroscopy. *J. Near Infrared Spectrosc.* **25**(5), 301–310 (2017).
45. Sirisomboon, P., Funke, A. & Posom, J. Improvement of proximate data and calorific value assessment of bamboo through near infrared wood chips acquisition. *Renew. Energy* **147**, 1921–1931 (2020).
46. Tsuchikawa, S. & Kobori, H. A review of recent application of near infrared spectroscopy to wood science and technology. *J. Wood Sci.* **61**, 213–220. <https://doi.org/10.1007/s10086-015-1467-x> (2015).
47. Yin, C.-Y. Prediction of higher heating values of biomass from proximate and ultimate analyses. *Fuel* **90**, 1128–1132 (2011).
48. Sirisomboon, P., Gyawali, P., Posom, J., Funke, A. & Shrestha, B. P. Possibility of NIR spectroscopy on non-destructive prediction of greenhouse gas emission by biomass combustion. In *Proceedings of the 10th International Conference on Green Energy Technologies (ICGET 2025), July 20–22, 2025, Nagasaki, Japan* (To appear in the Green Energy and Technology book series by Springer) (in press).
49. Gnoni, M. G., Elia, V. & Lettera, G. A strategic quantitative approach for sustainable energy production from biomass. *Int. J. Sustain. Eng.* **4**(2), 127–135. <https://doi.org/10.1080/19397038.2010.544420> (2011).

## Acknowledgements

The authors express their gratitude to School of Engineering, King Mongkut's Institute of Technology, Ladkrabang, the Near-Infrared Spectroscopy Research Center for Agricultural Product and Food ([www.nirsresearch.com](http://www.nirsresearch.com)), Department of Agricultural Engineering, School of Engineering at King Mongkut's Institute of Technology Ladkrabang, Thailand, for providing instruments and space for the experiment. They would also like to thank the Department of Research and Graduate studies, Khon Kaen University, Thailand for their research support. Additionally, the authors extend their appreciation to the Department of Mechanical Engineering, Kathmandu University, Nepal, for assisting in collecting biomass samples from various locations in Nepal. This research was funded by the School of Engineering, King Mongkut's Institute of Technology Ladkrabang, Thailand (Contract No: 2567-02-01-040).

## Author contributions

P.G. and B.S.: conceptualization, methodology, software, formal analysis, investigation, resources, data curation, writing the original draft, writing–review & editing, visualization. J.P.: conceptualization, software, formal analysis, writing–review & editing, supervision. B.P.S. and A.F.: conceptualization, writing the original draft, writing–review & editing, validation, supervision. P.P.: conceptualization, P.S.: conceptualization, methodology, writing the original draft, writing–review & editing, supervision, project administration, funding acquisition. All authors have read and agreed to the published version of the manuscript.

## Declarations

### Competing interests

The authors declare no competing interests.

### Additional information

**Correspondence** and requests for materials should be addressed to J.P. or P.S.

**Reprints and permissions information** is available at [www.nature.com/reprints](http://www.nature.com/reprints).

**Publisher's note** Springer Nature remains neutral with regard to jurisdictional claims in published maps and institutional affiliations.

**Open Access** This article is licensed under a Creative Commons Attribution-NonCommercial-NoDerivatives 4.0 International License, which permits any non-commercial use, sharing, distribution and reproduction in any medium or format, as long as you give appropriate credit to the original author(s) and the source, provide a link to the Creative Commons licence, and indicate if you modified the licensed material. You do not have permission under this licence to share adapted material derived from this article or parts of it. The images or other third party material in this article are included in the article's Creative Commons licence, unless indicated otherwise in a credit line to the material. If material is not included in the article's Creative Commons licence and your intended use is not permitted by statutory regulation or exceeds the permitted use, you will need to obtain permission directly from the copyright holder. To view a copy of this licence, visit <http://creativecommons.org/licenses/by-nc-nd/4.0/>.

© The Author(s) 2025